Structural and functional characterization of the antigenicity of influenza A virus hemagglutinin subtype H15

Disha Bhavsar[1,2,8], André Nicolás León[3,8], Wei-Li Hsu[4], Eduard Puente-Massaguer[1,2], James A. Ferguson[3], Julianna Han[3], Patrick Wilson[5], Andrew B. Ward[3], Florian Krammer[1,2,6,7]

[1]Department of Microbiology, Icahn School of Medicine at Mount Sinai, New York, New York, USA

[2]Center for Vaccine Research and Pandemic Preparedness (C-VaRPP), Icahn School of Medicine at Mount Sinai, New York, NY, USA

[3]Department of Integrative Structural and Computational Biology, The Scripps Research Institute, La Jolla, CA, USA

[4]Graduate Institute of Microbiology and Public Health, National Chung Hsing University, Taichung City, Taiwan

[5]Drukier Institute for Children's Health, Department of Pediatrics, Weill Cornell Medicine, New York, NY, USA

[6]Department of Pathology, Molecular and Cell Based Medicine, Icahn School of Medicine at Mount Sinai, New York, NY, USA

[7]Ignaz Semmelweis Institute, Interuniversity Institute for Infection Research, Medical University of Vienna, Vienna, Austria

[8]Co-first author

SUMMARY

Avian H15 influenza viruses are closely related to H7 viruses, but feature a unique 9-amino acid insertion in their hemagglutinin head domain, creating an additional site for antigenic variation. Here, we characterized a panel of mouse monoclonal antibodies (mAbs) raised against the A/wedge-tailed shearwater/Western Australia/2576/1979 ancestral strain, and a human mAb isolated from an H7N9 vaccinee. We found differences in binding and neutralization profiles against the ancestral strain and drifted strains of H15 isolated after 2008. MAbs that have hemagglutination inhibition activity against the ancestral strain do not show binding to drifted strains, hinting at antigenic differences in the receptor binding site. We show that the mAbs protect *in vivo* and elucidate mAb-antigen interactions using negative stain and cryo-electron microscopy. The characterization of H15 antigenicity and mechanisms of antibody-mediated

neutralization expands our knowledge of this rare avian influenza virus and informs our understanding of immune pressures on viral surface glycoproteins.

INTRODUCTION

Global climate change, habitat destruction and disruption, light pollution, and other human activities have caused physiological and behavioral changes in migratory birds (Carey, 2009; Dezfuli et al., 2022; Horton et al., 2023; Shipley et al., 2022; Wang et al., 2022; Zimova et al., 2021). These changes have often led to population and health declines as well as the intermingling of species that were formerly geographically distinct, creating the preconditions necessary for devastating viral incursions (Chen & Khanna, 2024). The dangers associated with such instances is highlighted by recent reports of H5N1 influenza A virus (IAV) outbreaks in brown skuas and gentoo penguins in South Georgia and the Falkland islands—wild bird populations in which H5N1 had not been detected previously (Banyard et al., 2024). While there is an extensive literature on seasonal and pandemic IAVs that circulate in human populations and avian IAVs with high pandemic potential, it is important to note that wild birds are also threatened by IAV pandemics, particularly when managing the fitness impacts of habitat disruption, dietary disruption, and changes in global weather patterns that generally outpace the speed of evolutionary adaptation (Boon et al., 2007; Hanmer et al., 2022; Kleyheeg et al., 2017; Sehgal, 2010). Thus, studies of rare wild bird IAV subtypes function as both proactive mitigation of potential human spillover events, which are expected to increase due to climate change, and extensions of an ethos of wildlife stewardship in the wake of manmade impacts on wild bird populations.

Hemagglutinin (HA) is a type-I viral fusion glycoprotein expressed as a homotrimer on the surface of influenza virions. Most HAs recognize sialic acid glycans as their host receptors and host specificity is thereby defined by the ability to bind moieties of α2,3-sialic acid (predominant in avian hosts) or α2,6-sialic acid (predominant in mammalian hosts)Nineteen influenza A virus HA subtypes(Karakus et al., 2024) have been identified in the animal reservoir of which H1, H2 and H3 have caused human pandemics so far(Krammer et al., 2018). A number of other virus subtypes—like H4, H5, H6, H7, H9 and H10—have caused zoonotic infections,(Claas et al., 1998; Gao et al., 2013; Huang et al., 2015; Kayali et al., 2011; Shi et al., 2013; To et al., 2014; Yuen et al., 1998). One of the rarest subtypes is the H15 HA. H15 is a group 2 influenza AH7 and H10 HA by an in its globular head domain, a feature not found in any other influenza virus HA subtype so far(Tzarum et al., 2017; Yang et al., 2020). H15N9 was first isolated in 1979 in Australia from a shearwater and a shelduck with additional isolations of H15N2, H15N8, and H15N9 in Australia in 1983 from ducks, terns, shelducks(Röhm et al., 1996; Sivay et al., 2013). A report from 1996 describes it as a new subtype(Röhm et al., 1996). After

a long hiatus, H15N4 was found in 2008 in a teal in Russia(Sivay et al., 2013) followed by detections of H15N7 in (Sivay et al., 2013), 2012 in Sweden (H15N5 in mallard ducks) and finally in 2015 in ducks (H15N9) in Bangladesh(El-Shesheny et al., 2018) (Figure 1A). H15 has not been detected in the Americas so far and it is unclear if its main reservoir are *Charadriiformes*, *Procellariiformes,* or *Anseriformes* and if this has changed over time. So far, no human infections have been identified and H15 antibody cross-reactivity (e.g. from H3N2 infections) in human serum is among the lowest of all subtypes—(Nachbagauer et al., 2017).

The Global Initiative on Sharing All Influenza Data (GISAID) only contains data for 22 H15Nx viruses (Figure 1B); given the increasing number of avian influenza sero-surveillance studies, this suggests that H15Nx viruses are rare amongst bird populations studied thus far (Hassan et al., 2020; Khare et al., 2021). There are conflicting reports on the pathogenicity of H15Nx viruses in mice and human cell lines. In one study, H15N9 failed to cause mortality or significant weight loss in mice while in another H15N1 was found to cause severe viral pneumonia and high mortality (El-Shesheny et al., 2018; Qi et al., 2014). Thus, it is likely that the HA-NA pairing as well as genotype and accessory non-structural proteins play a large role in determining the pathogenicity of H15-expressing viruses. Given the potential for IAVs to undergo genome reassortment during viral replication, the presence of mammalian virulence factors in certain H15Nx viruses emphasizes the value of proactive study to enhance pandemic preparedness. Here, we set out to test the antigenicity of H15 viruses using monoclonal antibodies (mAbs) raised against the H15 strain from 1979 as well as polyclonal sera raised in mice. We further characterized the identified mAbs regarding their mechanism of action, protective effect, and epitopes. Collectively, this study provides the first molecular characterization of H15 HA antigenicity, reports the first structures of mAbs against this rare subtype, and highlights the need for further work on antigenic profiling of rare avian IAV glycoproteins both in mammals and in their native hosts.

RESULTS

Monoclonal antibody generation

Previously, human mAb 07-5G01 was isolated from an individual who received two doses of a live-attenuated cold-adapted influenza A/Anhui/1/2013 (H7N9) vaccine followed by an inactivated virus vaccine boost 12 weeks later (Henry Dunand et al., 2016). Interestingly, mAb 07-5G01 exhibited neutralizing activity against the A/wedge-tailed shearwater/Western Australia/2576/1979 (A/wt shearwater/WA/2579/1979) (H15N9) virus and bound to recombinant H15 HA.

109 H15 reactive mouse mAbs were generated using a hybridoma based approach. Female
110 BALB/c mice were infected with a sublethal dose of the A/wt shearwater/WA/1979
111 (H15N5, A/PR/8/34 reassortant) virus and subsequently boosted with an inactivated
112 preparation of the same virus. Splenocytes of these mice were fused with the SP2/0
113 myeloma cells to generate hybridoma cells. The supernatants from these cells were
114 screened for binding to A/wt shearwater/WA/1979 recombinant H15 in an enzyme linked
115 immunosorbent assay (ELISA). Four antibodies, KL-H15-3G11 (IgG_{2a}), KL-H15-6F6
116 (IgG_{2a}), KL-H15-6G8 (IgG_{2a}) and KL-H15-6H4 (IgG_{2b}) were found to bind the recombinant
117 H15 and were selected for further characterization (Figure 1C).

118

119 **The isolated mAbs show limited reactivity to a panel of H15 hemagglutinins**

120 To determine the breadth of antigenic activity of the mAbs against a range of H15s, the
121 full length amino acid sequences of selected H15 sequences were aligned using Clustal
122 Omega and analyzed phylogenetically via neighbor-joining tree method (Figure 1D). The
123 sequence alignment revealed mutations in the putative major antigenic sites of the H15s,
124 some of which are consistent across the strains reported since 2008 (Figure 1E). ELISAs
125 were performed against a panel of recombinant H15 proteins from viruses spanning from
126 1979 to 2015, when the most recent H15 virus isolate was reported. While all five mAbs
127 bound to the recombinant H15 from the A/wt shearwater/WA/1979 strain, only KL-H15-
128 6H4 showed binding against the recombinant H15 from the strains reported since 2008
129 (Figure 2A). All mAbs showed binding in ELISA against recombinant chimeric 15/3
130 hemagglutinin (cH15/3) which consists of head domain from A/wt shearwater/WA/1979
131 H15 and stalk domain from A/Hong Kong/4801/2014 H3 (Chen et al., 2016), indicating
132 that all the mAbs potentially bind the head domain of H15 HA.

133 An immunofluorescence (IF) assay was also performed to test the binding of the mAbs to
134 H15 HAs expressed on the surface of infected cells in their native conformation.
135 Reassortant viruses (6:2) were generated with HA and NA from the A/wt
136 shearwater/WA/1979 (H15N9), A/teal/Chany/7119/2008 (H15N4), A/mallard
137 duck/Sweden/139647/2012 (H15N5), and A/duck/Bangladesh/24704/2015 (H15N9)
138 strains and the internal proteins from the A/PR/8/34 (H1N1) strain. A 7:1 reassortant virus
139 was generated for the A/mallard/Novomychalivka/2-23-12/2010 (H15N7) strain where NA
140 from A/PR/8/34 was used. Madin Darby canine kidney (MDCK) cells were infected with
141 the five different H15 virus strains and used for an IF assay. All mAbs showed high binding
142 intensity to cells infected with A/wt shearwater/WA/1979, while only KL-H15-6H4 showed
143 binding to cells infected with H15 strains isolated 2008 onwards, corroborating the results
144 observed in ELISA (Figure 2B). Similar results were observed in ELISA against purified
145 A/wt shearwater/WA/1979 H15N9 virus (Figure S1A).

146 Binding of these mAbs against A/wt shearwater/WA/1979 recombinant H15 was also
147 tested via Western blot following reducing denaturing sodium dodecyl sulfate
148 polyacrylamide gel electrophoresis (SDS-PAGE). All mAbs bound to H15 indicated by the
149 presence of bands on the Western blot, although 07-5G01 seemed to bind to a lesser
150 extent as indicated by the relatively low intensity of the band (Figure S1B).

151

152 **The majority of the isolated mAbs have neutralizing activity against the A/wt**
153 **shearwater/WA/1979 strain *in vitro***

154 To assess whether the mAbs can neutralize the H15 viruses *in vitro*, microneutralization
155 assays were performed. Even though the virus used to immunize the mice to generate
156 the hybridomas had a mismatched NA (A/wt shearwater/WA/1979 H15N5), all mAbs were
157 able to neutralize the A/wt shearwater/WA/1979 (H15N9) virus with minimal neutralizing
158 concentrations ranging from 1 µg/ml to 0.1 µg/ml (Figure 3A). Only KL-H15-6H4 showed
159 neutralization activity against A/teal/Chany/7119/2008 (H15N4),
160 A/mallard/Novomychalivka/2-23-12/2010 (H15N7), and A/mallard
161 duck/Sweden/139647/2012 (H15N5) viruses. None of the mAbs showed detectable
162 neutralization activity against A/duck/Bangladesh/24704/2015 (H15N9) virus at the
163 highest tested concentration.

164 To determine if the neutralization activity of these mAbs is driven by blocking of the
165 receptor binding site (RBS) of H15, a hemagglutination inhibition (HI) assay was used
166 (Brandenburg et al., 2013). KL-H15-3G11, KL-H15-6F6, KL-H15-6G8 and 07-5G01
167 showed HI activity against A/wt shearwater/WA/1979 (H15N9) at minimum HI
168 concentrations ranging from 0.94 µg/ml to 0.23 µg/ml (Figure 3B). While KL-H15-6H4 was
169 observed to have neutralization activity, no HI activity was detected for this mAb, hinting
170 at neutralization by mechanisms other than blocking of the RBS. No HI activity was
171 observed for these mAbs against the virus strains isolated since 2008 (Figure S1C).

172 In addition to microneutralization assays, the neutralization activity of these mAbs was
173 also tested in a plaque reduction neutralization assay (PRNA) against A/wt
174 shearwater/WA/1979 (H15N9) virus. Neutralization capacity was determined by the
175 percentage reduction in number of plaques formed by the virus incubated with dilutions
176 of the corresponding mAb compared to an irrelevant IgG. All mAbs showed 100%
177 reduction in plaque number at the highest tested concentration of 100 µg/ml. The 50%
178 inhibitory concentration (IC_{50}) values were 0.11 µg/ml for KL-H15-3G11, 0.17 µg/ml for
179 KL-H15-6F6, 0.001 µg/ml for KL-H15-6G8, 8.039 µg/ml for KL-H15-6H4 and 0.52 µg/ml
180 for 07-5G01 (Figure 3C).

181 Interestingly, reduction in plaque size was also observed in the wells treated with
182 neutralizing mAbs in addition to reduction in number of plaques (Figure S2A). HA mAbs

183 have previously been shown to inhibit neuraminidase activity and contribute to influenza
184 virus neutralization due to steric hindrance (Rajendran et al., 2017; Wohlbold et al., 2016).
185 To assess this, neuraminidase inhibition (NAI) assays were performed using an enzyme-
186 linked lectin assay (ELLA). MAbs were pre-incubated with A/wt shearwater/WA/1979
187 (H15N9) and transferred onto fetuin coated plates. Cleavage of sialic acid was measured
188 by binding of peanut agglutinin. No virus and no mAb controls were used to normalize
189 100% and 0% neuraminidase NA inhibition. Mab 1G01, a broadly cross-reactive anti-
190 influenza virus neuraminidase antibody was used as a positive control (Stadlbauer et al.,
191 2019). At the maximum tested concentration of 30 µg/ml, the mAbs appeared to show
192 50% NA inhibition (Figure 3D). KL-H15-6H4 was also able to inhibit the neuraminidase
193 NA activity of H15 viruses isolated 2008 onwards (Figure S2B). Additionally, all mAbs
194 except 07-5G01 were also able to induce varying degrees of detectable antibody-
195 dependent cellular cytotoxicity (ADCC) activity when measured using a commercial
196 reporter assay (Figure S2C).

197

198 **The mAbs confer protection *in vivo* against lethal H15 virus challenge and inhibit**
199 **viral replication in mouse lungs**

200 *In vivo* protective efficacy of the mAbs was tested in a mouse model against lethal
201 challenge with A/wt shearwater/WA/1979 (H15N5) virus in a prophylactic setting. MAbs
202 were administered intraperitoneally at either 10 mg/kg, 2 mg/kg or 0.1 mg/kg dose in
203 female BALB/c mice 2 hours prior to intranasal challenge with 5 murine 50% lethal doses
204 (mLD_{50}) of A/wt shearwater/WA/1979 (H15N5) virus. At the 10 mg/kg dose, 100% survival
205 was observed with all mAbs. Most mAbs were also completely protective at the 2 mg/kg
206 dose, except KL-H15-3G11, for which 80% of the mice survived. MAbs KL-H15-6G8 and
207 07-5G01 were able to confer partial protection (40% survival) even at the 0.1 mg/kg dose,
208 however weight loss was more pronounced in these groups compared to the ones treated
209 with higher doses of the same mAbs (Figure 4A).

210 In addition to protection, the ability of the mAbs to inhibit viral replication in lungs of mice
211 challenged with H15 virus was also tested. MAbs were administered at 10 mg/kg dose
212 intraperitoneally in female BALB/c mice which were then challenged with 1 mLD_{50} of A/wt
213 shearwater/WA/1979 (H15N5) virus. Lungs of these mice were harvested at 3 and 6 days
214 post infection (DPI) and viral load was assessed using plaque assay. No replicating virus
215 was detected in the lungs of mice treated with all mAbs at either time points (Figure 4B).
216 This is consistent with the *in vivo* protection experiment and, combined with the results of
217 neutralization assays, suggests that virus neutralization might be the primary mechanism
218 of protection.

219 **Structural characterization demonstrates mAbs cluster into three distinct binding**
220 **classes**

Although KL-H15-6H4 and 07-5G01 were recalcitrant to negative stain electron microscopy, reconstructions of KL-H15-6G8, KL-H15-3G11, and KL-H15-6F6 revealed that all three mAbs targeted the H15 HA head (Figure S3). Sequence alignments highlighted shared and distinct features utilized by the mAbs in this study: KL-H15-6H4 and KL-H15-6F6 shared similar light-chains; KL-H15-3G11, KL-H15-6G8, and KL-H15-6H4 shared similar heavy-chains; and KL-H15-3G11 and KL-H15-6G8 shared similar light-chains (Figure S4). To characterize the relationship between complementarity-determining region (CDR) sequences and antigen engagement and to interrogate how KL-H15-6H4 was uniquely able to neutralize strains isolated after 1979, structures of A/wt shearwater/WA/2576/1979 H15 HA complexes were obtained using cryo-electron microscopy (Figure 5, Table S1).

As suggested by their nearly identical light- and heavy-chain CDRs, KL-H15-3G11 and KL-H15-6G8 engaged A/wt shearwater/WA/2576/1979 H15 HA in a nearly identical manner, utilizing a series of aromatic and polar uncharged residues to form a network of hydrogen bonds with H15 HA residues in or near the 130-loop, 150-loop, and 190-helix (Figure 5A-D, Figure S5A-B, Table S2). Given their similarity, KL-H15-3G11 and KL-H15-6G8 were grouped into Class 1. All heavy-chain CDRs and CDRL1 and 3 of Class 1 mAbs were involved in antigen engagement (Figure 5C). Atomic modeling of KL-H15-6G8 showed 3 hydrogen bonds formed between H15 HA and CDRL1 and CDRL3 and at least 5 formed with CDRH1, CDRH2, and CDRH3 (Fig 5D). The heavy-chain CDRs engaged residues N166, N167, Q168, and T206. Q27 in CDRL1 and E93 in CDRL3 formed hydrogen bonds with S136 and G137, respectively while T28 in CDRL1 formed a backbone-to-backbone hydrogen bond with Q172. Hydrophobic interactions between P171 on the H15 HA protomer and Y32 in CDRL1 and W92 in CDRL3 were also identified (Figure 5D).

07-5G01 engaged the H15 HA trimer in a distinct fashion and is defined as a Class 2 mAb (Figure 5E, F, Figure S5C). In 07-5G01, rather than forming a hydrophobic interaction with P171, W94 in CDRL3 formed a hydrogen bond with N167 analogous to the interaction between N167 and CDRH1 W33 in KL-H15-6G8 and KL-H15-3G11 (Figure 5G). Y32 in CDRL1 forms a pi-cation interaction with R139 rather than a van der Waals interaction with P171. In the heavy-chain, S52A in CDRH2 forms a side-chain-to-side-chain hydrogen bond with S136 while D53, Y58, and Y100D form side-chain-to-back-bone hydrogen bonds with residues S163, V169, and I138, respectively.

Unlike Class 1 and 2 mAbs, KL-H15-6H4 binds towards the center of the trimer, extending the antibody footprint towards the protomer-protomer interface (Figure 5H-I, Figure S5D). In KL-H15- 6H4, antigen engagement is primarily mediated by CDRL1 and CDRH2 (Figure 5J). Q29 and S27E in CDRL1 both form side-chain-to-side-chain hydrogen bonds with D198 while Y32 forms a hydrogen bond with the side-chain of N201. S206 and G207 on the HA trimer form hydrogen bonds with the backbones of residues Y91 and H92 in

CDRL3, respectively. Like 07-5G01, the KL-H15-6H4 heavy-chain CDRs directly interact with V169 and S163, the former through hydrophobic interactions with W32 in CDRH1 and the latter through side-chain hydrogen bonding with N54 in CDRH2. Like Q27 in 6G8 CDRL1, Y52 in KL-H15-6H4 CDRH2 forms a hydrogen bond with G137 with an additional bond formed with S164. Lastly, D52 in CDRH2 forms a hydrogen bond with the backbone of Q172. Although CDRH3 was not predicted to make prominent contacts with antigen, it should be noted that the Y97 and Y100 sidechains in KL-H15-6H4 CDRH3 were not built into the map as there was insufficient density to do so with confidence. This may be the result of high flexibility in the region at this angle of approach. While we were unable to build an atomic model for KL-H15-6F6, docking of the predicted variable fragment (Fv) revealed that contacts with the H15 trimer were mediated by CDRH1, CDRH2, and CDRL3 (Figure S5E, Figure S6). As the KL-H15-6F6 light chain variable regions are nearly identical to that of KL-H15-6H4, this observation suggests that the contacts mediated by the KL-H15-6F6 heavy chain lead to rearrangement of the Fab angle of approach such that the CDRL1 contacts observed in KL-H15-6H4 play a less critical role in antigen engagement.

Structural analysis of antigen engagement by H15 sequence conservation and putative antigenic sites revealed that all three mAb classes engage distinct but overlapping footprints on the H15 head (Figure 6A). All three classes engage primarily with major antigenic site B. All heavy-chain contacts made by Class 1 mAbs engaged residues in site B, while E93 in CDRL3 formed a hydrogen-bond with G137, which is present in both sites A and B. 07-5G01 formed direct contacts with residues in site B, but engaged with residues S136 and I138 which straddle G137 in site A and may be able to flexibly engage with R134 in putative site E. While still primarily engaging with site B residues, the KL-H15-6H4 footprint extends towards the protomer-protomer interface and incorporates a greater number of absolutely conserved residues relative to Class 1 and 2 mAbs. Our structural models reveal that the emergence of M165R/K and N166 mutations in strains isolated after 1979 would sterically hinder and/or charge repulse engagement by Class 1 mAbs, which directly interact with residues N166 and N167, and 5G01 which interacts with residue N167 (Figure 5D and G). Associated rearrangement of neighboring residues may also contribute to loss of binding and neutralization. While KL-H15-6H4 engages spatially adjacent residues, it does not form key hydrogen bonds with N166 or N167 thereby preserving binding to strains through A/duck/Bangladesh/24704/2015 (H15N9) and neutralization through A/mallard duck/Sweden/336472/2012 (H15N5) (Figure 2A, Figure 5J).

Epitope mapping via escape mutagenesis

297 Given the difference in binding and neutralization activity of these mAbs against different
298 H15 viruses tested, determining the target epitopes for these mAbs can provide insights
299 into the evolution of H15 viruses. For the mAbs with HI activity, this was carried out in
300 specific pathogen free (SPF) embryonated chicken eggs in a single passage in the
301 presence of 250 µg of respective mAbs. 10^6 plaque forming units (PFU) of A/wt
302 shearwater/WA/1979 (H15N9) virus were incubated with either KL-H15-3G11, KL-H15-
303 6F6, KL-H15-6G8 or 07-5G01 and injected into 10 days old embryonated chicken eggs.
304 The allantoic fluid was harvested and screened for loss of HI activity to confirm escape.
305 The escape mutants were plaque purified on MDCK cells, grown in embryonated chicken
306 eggs and the HA segments were sequenced to identify the escape mutations. For KL-
307 H15-6H4, which has been shown to be neutralizing but HI inactive, escape mutagenesis
308 was done by sequential passaging of A/wt shearwater/WA/1979 (H15N9) virus with the
309 mAb starting at $0.5xIC_{50}$ and doubling the concentration at every passage up to $128xIC_{50}$.
310 The resultant viruses were screened for loss of binding, and thus escape, by
311 immunofluorescence assay. The viruses were then plaque purified on MDCK cells, grown
312 in embryonated chicken eggs and the HA segments were sequenced . Interestingly, the
313 same G137E mutation was observed in the mutant viruses that escaped from KL-H15-
314 3G11, KL-H15-6F6 and KL-H15-6G8, while an S163F mutation was identified in KL-H15-
315 6H4 escape mutants and 07-5G01 escape mutant carried the Q168K mutation (Figure
316 6B, C). Both S163F and Q168K mutations are within the putative antigenic site B of the
317 H15 HA, while the G137E mutation is within the putative antigenic site A. These findings
318 further corroborate the neutralization potential of these mAbs. While these particular
319 residues are conserved across different H15s tested in this study, there are several
320 mutations in the regions flanking these sites which might explain the difference in binding
321 and neutralization profile of these mAbs. Our structural models also clarify the molecular
322 basis of escape mutations identified in this study: G137E (Class 1), Q168K (Class 2), and
323 S163F (Class 3) (Figure 6B-C). G137E may disrupt hydrogen bonding between residues
324 G137 in the trimer and E93 in CDRL1 and may introduce steric clashes with residue W92.
325 Similar to the naturally occurring M165R/K and N166 mutations, Q168K introduces a
326 large, positively-charged residue into a polar uncharged pocket, potentially creating steric
327 clashes and disrupting hydrogen bonding networks mediated by W94 in CDRL3 and
328 Y58in CDRH2. In contrast, S163F does not directly interfere with residues in the KL-H15-
329 6H4 paratope, but analysis of steric clashes suggests that it may disrupt the epitope
330 pocket and thereby ablate neutralization.

331

332 **Polyclonal serum responses to different H15 viruses indicate antigenic drift**

333 The remarkable difference in the binding and neutralization activity of the mAbs tested in
334 this study, particularly the mAbs that have HI activity against A/wt shearwater/WA/1979
335 (H15N9) virus hint at antigenic differences between H15 viruses isolated in different

336 years. This can be further illuminated with the help of polyclonal responses to different
337 H15 viruses. Groups of female BALB/c mice were infected with different H15 viruses, sera
338 were collected 21 DPI and analyzed in an HI assay against both homologous and
339 heterologous H15 viruses. No detectable HI response was observed against the
340 homologous strain in sera obtained from mice infected with A/wt shearwater/WA/1979
341 (H15N9), hence the same mice were infected a second time, sera were collected 7 DPI
342 and used for the HI assay. Remarkable differences were observed between serum HI
343 reactivity against homologous and heterologous H15 viruses. Most noticeably, the sera
344 from mice infected with A/wt shearwater/WA/1979 (H15N9) showed a significant drop in
345 HI activity against newer H15 viruses (Table 1). This is similar to the pattern observed
346 with the HI-active mAbs from the panel and further hints at major antigenic differences
347 between the H15 from the 1979 reference strain to the most recent strain isolated in 2015.

348

349 **DISCUSSION**

350 The H15 subtype of influenza A virus has rarely been detected and has so far only been
351 found sporadically in Australia and Eurasia (El-Shesheny et al., 2018; Muzyka et al., 2012;
352 Röhm et al., 1996; Sivay et al., 2013). Here, we investigated the antigenicity of this
353 subtype and its different isolates using both mAbs and polyclonal serum.

354 MAbs generated to the prototype strain from a shearwater in 1979 which bound to putative
355 antigenic sites A and B (as compared with H3 HA) rapidly lost binding and neutralizing
356 activity to newer H15 virus isolates. Similarly, cross-reactivity of isolate specific sera in HI
357 assays was relatively poor. MAbs showed strong neutralization and HI activity and
358 protected mice potently from an H15 infection. The exception was mAb KL-H15-6H4
359 which had no HI activity but was the only mAb that showed breadth and bound to all
360 tested viruses. This mAb had neutralizing activity (despite not being HI active) and also
361 robustly protected mice from H15 virus challenge. These results suggest substantial
362 antigenic drift over time, which is noteworthy since this subtype is only detected rarely –
363 suggesting limited circulation, at least in sampled species.

364 While putative sites A and B on H15 correlate well with their H3 counterparts, sites C, D,
365 and E do not map onto H15 so analogously (Figure 6A). Putative sites C and E are
366 spatially discontiguous and over half of residues in putative site D are buried in relatively
367 inaccessible regions of the protomer-protomer interface. Analysis of variation in known
368 H15 HA sequences may offer insights into how to better characterize antigenic variation
369 in this related but rare and distinct subtype. Notably, multiple sequences collected from
370 Australian ducks in 1983 contain clusters of amino acid mutations in or near putative
371 antigenic sites D and E that are not observed before or after: A228D (site D), T180N (site
372 D proximal), L86K (site E), and S130P (site E). All except T180N constitute mutations that
373 introduce an electric charge or remove a polar side chain and all except L86K are within

374 or near well-characterized structural features also present in H7 and H10 HAs: loop-220,
375 helix-190, and loop-130 (Tzarum et al., 2017; Yang et al., 2020)In addition to these
376 mutations unique to 1983 strains, D57N (site C), K202Q (site B), and B151G (site A) are
377 observed across virtually all strains reported after 1983—A/mallard/Novomychalivka/2-
378 23-12/2010 being the exception as it lacks V151G. While it cannot be stated
379 unambiguously, the location of these mutations and relatively large changes in side chain
380 chemistry are suggestive of substantial immune pressure and antigenic drift.

381 Despite the variation observed in viral isolates at putative sites C, D, and E, all mAbs in
382 this study exclusively engage sites A and B, and primarily site B. Although it has been
383 observed that natural infection with H7N9 viruses in humans can induce antibody
384 responses to sites A, B, the HA stem, and the trimer interface, site B is dominant in human
385 antibody responses to circulating H3N2 strains (Gilchuk et al., 2021; Li et al., 2019;
386 Popova et al., 2012; Wu et al., 2020). While there have been several studies on the
387 immunogenicity of H7 and H10 in mice and ferrets, they primary utilize serological
388 techniques that do not disambiguate the relative immunodominance of major antigenic
389 sites (Bahl et al., 2017; Fadlallah et al., 2020; Kamal et al., 2017). Thus, it is unclear
390 whether the site A and B dominance observed in this study is generalizable to H7 and
391 H10 as well or if it is a feature of mouse immunization with the A/wt
392 shearwater/WA/2576/79 (H15N5) strain.

393 This is a salient question, as there is a paucity of data characterizing the molecular basis
394 of antibody responses to avian IAVs in wild or domesticated birds due to challenges
395 inherent in working in such systems. There are multiple reasons to believe that studies of
396 mammalian antibody responses to avian influenza viruses—and other avian pathogens
397 for that matter—may not reflect avian responses: 1) the primary immunoglobulin in birds
398 is IgY, which is related to but distinct from IgG; 2) in birds, IAV is primarily a gastrointestinal
399 disease and thus the avian immune response and particularly the avian mucosal immune
400 response likely relies on local T and B cell populations that are distinct from those involved
401 in the mammalian response to respiratory IAV infections; and 3) as the natural reservoirs
402 for IAVs, birds may experience repeat infections and thus studies of their antibody
403 responses and/or potential vaccination strategies may be needed to overcome the
404 challenge of pre-existing immunity (Causey & Edwards, 2008; Dascalu et al., 2024; Hill
405 et al., 2016; Leslie & Clem, 1969; Meade et al., 2017; Spackman, 2009; Vandegrift et al.,
406 2010; Zhang et al., 2017). Increasing our understanding of the immune pressures on
407 avian IAVs will be an essential component of efforts to vaccinate critically endangered
408 wild birds, as has already been attempted with the California condor (Katzner et al., 2025).

409 While influenza viruses mutate and change over time, significant changes are often driven
410 by evolutionary pressure such as a switch in host species and adaptation to the new
411 species or reinfection of hosts (meaning neutralizing antibodies are present that exert
412 pressure on the virus). It is unclear which mechanisms led to these significant antigenic

changes in H15 viruses. Furthermore, the rare detection suggests low prevalence, but the antigenic changes suggest that the virus is circulating in a larger reservoir. What this reservoir is, needs to be determined. However, it is clear that the virus is not widespread in *Charadriiformes*, *Procellariiformes* or *Anseriformes* due to the rare detections. Potentially, viruses detected in these birds are an indication of spill-over events from the real reservoir.

We believe our study sheds some light on this rare influenza A subtype – even though it raises several questions that need to be answered. Furthermore, the produced mAbs, recombinant proteins and re-assortant virus represent a set of reagents for the influenza virus research community to better study historic and future H15 viruses.

RESOURCE AVAILABILITY

Lead contact

Requests for information or reagents should be directed to Florian Krammer (florian.krammer@mssm.edu).

Materials availability

mAbs and plasmids for mAb expression can be obtained from the authors upon reasonable request.

Data and code availability

- CryoEM maps and models were deposited in the Electron Microscopy DataBank under accession IDs EMD-71419, EMD-71420, EMD-71421, EMD-71422, and EMD-71424, and in the Protein DataBank under accession IDs 9P9Q, 9P9R, 9P9S, and 9P9T (Table S1).
- The published article contains all datasets analyzed during the study.
- This paper does not report original code.
- Any additional information required to reanalyze the data reported in this paper is available from the lead contact upon request.

ACKNOWLEDGEMENTS

This work was also partially funded by the Centers of Excellence for Influenza Research and Response (CEIRR, contract #75N93021C00014, reagent generation), the Collaborative Influenza Vaccine Innovation Centers (CIVIC, National Institute of Allergy and Infectious Diseases contract #75N93019C00051), and by institutional funds. E.P.M. was also supported by a postdoctoral fellowship from Fundación Ramón Areces. We

thank Paul E. Leon for pilot study work on these mAbs. We thank Jesse Bloom for making his HA renumbering algorithm publicly available and the Bacterial and Viral Bioinformatics Resource Center (BV-BRC) for hosting it on an accessible user interface.

AUTHOR CONTRIBUTIONS

D.B. and F.K. designed the study. D.B. and A.L. designed and performed the experiments and analyzed data. W.H., and E.P.M. performed experiments and/or generated reagents. P.C.W. provided reagents. J.H., A.B.W. and F.K. supervised the study. D.B., A.L. and F.K. drafted the manuscript. All authors reviewed, edited and approved the final version of the manuscript.

DECLARATION OF INTERESTS

The Icahn School of Medicine at Mount Sinai has filed patent applications relating to SARS-CoV-2 serological assays, NDV-based SARS-CoV-2 vaccines influenza virus vaccines and influenza virus therapeutics which list Eduard Puente-Massaguer and Florian Krammer as co-inventor. Mount Sinai has spun out a company, Kantaro, to market serological tests for SARS-CoV-2 and another company, Castlevax, to develop SARS-CoV-2 vaccines. Florian Krammer is co-founder and scientific advisory board member of Castlevax. Florian Krammer has consulted for Merck, GSK, Curevac, Sanofi, Gritstone, Seqirus and Pfizer and is currently consulting for 3rd Rock Ventures and Avimex. The Krammer laboratory is also collaborating with Dynavax on influenza vaccine development and with VIR on development of antiviral mAbs.

FIGURE TITLES AND LEGENDS

Figure 1: Background to H15. (A) Global map showing the locations and the years during which H15 virus strains were reported. (B) Proportion of different virus subtypes with H15 HA. Sequences of influenza virus strains with H15 HA subtype were obtained from Global Initiative on Sharing All Influenza Data (GISAID) and classified based on the NA subtype. (C) mAbs used in the study along with the source from which they were isolated. 07-5G01 was isolated from a human subject vaccinated against H7N9 virus (Henry Dunand et al., 2016), whereas the other mAbs were obtained from murine hybridomas generated by immunization with H15N5 virus. (D) The phylogenic tree representing the antigenic distance between different H15 HAs used in the study. The scale bar represents a 3% amino acid difference in sequence identity. The sequences were obtained from GenBank, and the phylogenetic tree was generated using Clustal Omega and visualized using FigTree. (E) Alignment of H15 sequences showing major

483 antigenic sites. The amino acid sequences obtained from GenBank were aligned using
484 Clustal Omega, and the sequences corresponding to the major antigenic sites are
485 represented. The amino acid differences are marked with asterisks.

486 **Figure 2: Binding of mAb panel to different H15 HAs**. (A) Binding profile of mAbs to
487 recombinant H15s from 1979 to 2015 and cH15/3 proteins as assessed by ELISA. The
488 broadly cross-reactive HA antibody CR9114 (Dreyfus et al., 2012) was used as a positive
489 control and anti-H6 antibody KL-H6-8H9 was used as negative control. (B) Binding of
490 mAbs to cells expressing H15 HA. Binding of mAbs to MDCK cells infected with different
491 H15 viruses and thus, expressing H15 on cell surface, was assessed by
492 immunofluorescence. CR9114 (Dreyfus et al., 2012) was used as a positive control and
493 anti-H6 antibody KL-H6-8H9 was used as negative control.

494 **Figure 3: In vitro neutralization of H15 viruses by mAbs**. (A) Neutralizing activity of
495 mAbs against different H15 viruses measured by microneutralization assay. Shown here
496 are the minimum concentrations of mAbs at which virus neutralization was observed.
497 Broadly neutralizing HA antibody CR9114 (Dreyfus et al., 2012) was used as a positive
498 control and anti-H6 antibody KL-H6-8H9 was used as a negative control. (B) HI activity
499 of mAbs against A/wt shearwater/WA/2576/1979 virus. The ability of the mAbs to
500 neutralize the virus via blocking the receptor binding site of H15 was assessed by HI
501 assay and the minimum concentration at which HI activity was observed is shown here.
502 Anti-H6 antibody KL-H6-8H9 was used as negative control. (C) Neutralizing activity of
503 mAbs against A/wt shearwater/WA/2576/1979 virus measured by PRNA. Percentage
504 reduction in number of plaques for each mAb, in five-fold dilutions starting at 100ug/ml,
505 is shown here normalized to negative control mAb KL-H6-8H9. (D) NAI activity of mAbs
506 against A/wt shearwater/WA/2576/1979 virus. Neuraminidase inhibition activity of the
507 mAbs was measured by ELLA. Virus only and no-virus controls were used to normalize
508 0% and 100% neuraminidase inhibition activity, broadly cross reactive influenza virus
509 neuraminidase antibody 1G01 (Stadlbauer et al., 2019) was used as a positive control,
510 while anti-H6 antibody KL-H6-8H9 was used as negative control.

511 **Figure 4: Protective efficacy of mAbs against lethal challenge *in vivo***. (A) Protection
512 against lethal challenge in mice. Five mice per group were given mAbs intraperitoneally
513 at a dose of 10 mg/kg, 2 mg/kg or 0.5 mg/kg and 2 hours later, they were challenged with
514 5 mLD_{50} of A/wt shearwater/WA/2576/1979 (H15N5) intranasally. Weight loss was
515 monitored for 14 days post challenge and the mean weight loss for each group is shown,
516 with error bars representing standard deviation. Survival plots for the same duration are
517 shown. (B) Viral lung titers after infection with A/wt shearwater/WA/2576/1979 (H15N5)
518 virus. Six mice per group were given mAbs intraperitoneally at 10 mg/kg and 2 hours later,
519 challenged with 1 mLD_{50} of A/wt shearwater/WA/2576/1979 (H15N5) intranasally. Mice
520 were euthanized on day 3 and day 6 post infection, the lungs were harvested and viral
521 titer in lung homogenates was determined using plaque assay.

522 **Figure 5. Structural characterization of Class 1, 2, and 3 epitope-paratope**
523 **interactions.** (A) KL-H15-6G8 and KL-H15-3G11 EM maps used for model building. (B-
524 C) Superimposed models of KL-H15-6G8 and KL-H15-3G11 in complex with A/wt
525 shearwater/WA/2576/1979 H15 HA highlight a shared binding mode. KL-H15-6G8
526 depicted in shades of red and KL-H15-3G11 in shades of blue. Heavy chains depicted in
527 darker shades and light chains in lighter shades. The 130-loop, 150-loop, and 190-helix—
528 antigenic regions shared with H3 HA—are depicted in shades of purple. (D) Zoomed view
529 of light- and heavy-chain contact sites conserved across both KL-H15-6G8 and KL-H15-
530 3G11 depicted as sticks using the KL-H15-6G8 model. Hydrogen bonds illustrated as
531 dashed lines. All antibodies presented in Kabat numbering. (E-F) Map and model for 07-
532 5G01 mAb binding. (G) 07-5G01 light- and heavy-chain contact sites presented as sticks
533 with hydrogen bonds illustrated as dashed grey lines and a pi-cation interaction depicted
534 as a light-blue dashed line. (H-I) Map and model for KL-H15-6H4 mAb binding. (J)
535 Zoomed view of light- and heavy-chain contact sites.

536 **Figure 6. Structural analysis of mAb binding.** (A) Top-view of the A/wt
537 shearwater/WA/2576/1979 H15 trimer; bound protomer presented in light grey. Dashed
538 lines are used to demarcate the footprints—defined as residues within 5Å of Fabs—for
539 Class 1 in red, Class 2 in orange, and Class 3 in green. Bound protomer is colored by
540 conservation across all 22 unique H15 sequences with degree of variability increasing
541 from white to teal. Putative major antigenic sites are presented and color coded: Site A
542 (red), B (blue), C (green), D (orange), and E (purple). The receptor binding site is
543 highlighted in yellow. (B) Location of escape mutations derived from viral passage are
544 depicted on a model of a A/wt shearwater/WA/2576/1979 H15 trimer. (C) Zoomed in
545 views of escape mutations separated by antibody class. Mutations were modeled in
546 ChimeraX and the top ten most prevalent rotamers are presented as sticks in grey. Steric
547 clashes with paratope residues are depicted using purple dashed lines.

548

549 **Table 1. Serum HI cross reactivity:** The values represent the last reciprocal dilution of
550 sera at which HI activity was observed. Median values are shown in bold font, followed
551 by the range in parenthesis.

Strain used to infect mice	**Strain used in HI assay**				
	A/wt shearwater/ WA/	**A/teal/Chany/ 7119/2008**	**A/mallard/ Novomychalivka/ 2-23-12/2010**	**A/mallard duck/ Sweden/**	**A/duck/ Bangladesh/**

	2576/1979			**139647/2012**	**24704/2015**
A/wt shearwater/ WA/2576/1979	**20** (10-20)	**5** (5-10)	**5** (5-10)	**5** (5-10)	**5** (5-10)
A/teal/Chany/ 7119/2008	**10** (5-10)	**80** (80-80)	**160** (80-160)	**40** (5-80)	**10** (10-40)
A/mallard/ Novomychalivka/ 2-23-12/2010	**10** (5-10)	**20** (10-80)	**320** (160-320)	**40** (10-40)	**20** (10-40)
A/mallard duck/Sweden/ 139647/2012	**5** (5-5)	**5** (5-10)	**5** (5-20)	**40** (40-40)	**5** (5-10)
A/duck/ Bangladesh/ 24704/2015	**5** (5-5)	**10** (5-160)	**20** (10-160)	**40** (20-160)	**160** (40-320)

STAR Methods

Experimental model and study participant details

Mab 07-5G01 was generated from the sequences obtained from plasmablasts isolated from an individual who received two doses of a live-attenuated cold-adapted influenza A/Anhui/1/2013 (H7N9) vaccine followed by an inactivated virus vaccine boost 12 weeks later. The details of the sample collection are described in a previous publication: Henry Dunand, Carole J et al. “Both Neutralizing and Non-Neutralizing Human H7N9 Influenza Vaccine-Induced Monoclonal Antibodies Confer Protection.” Cell host & microbe vol. 19,6

562 (2016): 800-13. doi:10.1016/j.chom.2016.05.014 PMCID: PMC4901526 NIHMSID:
563 NIHMS789757 PMID: 27281570.

564

565 **Cells, viruses and recombinant glycoproteins**

566 Dulbecco's modified Eagle's medium (DMEM; Gibco) supplemented with Pen-Strep
567 antibiotic solution (penicillin at 100 U/ml and streptomycin at 100 µg/ml; Gibco), 10 ml of
568 1 M 4-(2-hydroxyethyl)-1-piperazineethanesulfonic acid (HEPES; Life Technologies) and
569 10% fetal bovine serum (FBS; Gibco) was used to culture MDCK (ATCC# CCL34) and
570 human embryonic kidney 293T (HEK-293T; ATCC# CRL-3216) cells in a 37°C incubator
571 with 5% CO_2. Expi293 medium (Gibco) was used to culture Expi293F (Gibco# A14527)
572 cells in suspension culture shaking at 125 RPM in an incubator at 37°C and 8% CO_2.
573 Hybridoma clones were initially cultured in ClonaCell-HY Medium E (Stemcell
574 Technologies) and progressively switched to culture in hybridoma-serum free medium
575 (Hybridoma-SFM; Gibco). *Spodoptera frugiperda* (Sf9) cells were grown in TNM-FH
576 insect medium (Gemini Bio) supplemented with 10% FBS and antibiotics (100 U/ml of
577 penicillin, 100 µg/ml streptomycin; Gibco). BTI-TN-5B1-4 (Trichoplusia ni) cells were
578 grown in serum-free Sf-900 II medium (Gibco) supplemented with antibiotics (100 U/ml of
579 penicillin, 100 µg/ml streptomycin; Gibco).

580 HA and NA sequences from the following isolates were obtained from GenBank and were
581 commercially synthesized (Genewiz; Azenta Life Sciences): A/wt
582 shearwater/WA/2576/1979 (H15N9; CY006010 and CY005407), A/teal/Chany/7119/2008
583 (H15N4; CY098540 and CY098542), A/mallard/Novomychalivka/2-23-12/2010 (H15N7;
584 KP087869), A/mallard duck/Sweden/139647/2012 (H15N5; MF147992 and MF148018)
585 and A/duck/Bangladesh/24704/2015 (H15N9; KY635680 and KY635500). Recombinant
586 H15 viruses were rescued with the HA and NA from the original isolate and the remaining
587 six segments from A/PR/8/34 (A/PR/8/34, H1N1) as 6:2 reassortant viruses using the
588 protocol described previously (Martínez-Sobrido & García-Sastre, 2010). The A/PR/8/34
589 backbone is attenuated in humans and generally considered safe (Beare et al., 1975).
590 A/mallard/Novomychalivka/2-23-12/2010 (H15N7) virus was rescued with HA from the
591 original isolate and the remaining seven segments from A/PR/8/34 as 7:1 reassortant
592 virus, as the NA sequence from the original isolate is incomplete. A/wt
593 shearwater/WA/2576/1979 (H15N5) mouse challenge virus was rescued using NA
594 sequence from A/mallard/Sweden/86/2003 (H12N5; GenBank accession: CY060392.1).
595 Virus stocks were grown in SPF-embryonated chicken eggs for 48 hours at 37°C followed
596 by harvest of allantoic fluid and clarification by centrifugation at 300x*g* for 5 minutes. The
597 virus stocks were stored at -80°C before use.

598 A/wt shearwater/WA/2576/1979 purified virus preparation for ELISA was made by low-
599 speed centrifugation of allantoic fluid to remove debris (300 × g at 4°C for 5 minutes),

600 followed by ultracentrifugation at 25,000 rpm for 2 hours at 4°C with an SW-28 rotor in a
601 Beckman L7-65 ultracentrifuge through a 30% sucrose cushion buffered with NTE buffer
602 (100 mM NaCl, 10 mM Tris-HCl, and 1 mM ethylenediaminetetraacetic acid EDTA
603 balanced to pH 7.4). The supernatant containing allantoic fluid was aspirated, and the
604 pellet was resuspended in phosphate buffered saline (PBS).

605 Recombinant HA proteins were expressed and purified using a mammalian expression
606 system as previously described (Sano et al., 2021). Briefly, the ectodomains of HA
607 proteins from A/wt shearwater/WA/2576/1979 (H15N9), A/teal/Chany/7119/2008
608 (H15N4), A/mallard/Novomychalivka/2-23-12/2010 (H15N7), A/mallard
609 duck/Sweden/139647/2012 (H15N5) and A/duck/Bangladesh/24704/2015 (H15N9) were
610 cloned into a pCXSN vector containing thrombin cleavage site, a foldon T4 trimerization
611 domain and a hexa-histidine tag, and transiently transfected into Expi293F cells using an
612 Expi293 transfection kit per the manufacturer's instructions. The supernatant was
613 collected 7 days post transfection and purified using affinity purification with nickel-
614 nitrilotriacetic acid (Ni-NTA) agarose beads (Qiagen). Recombinant H1 from A/PR/8/34
615 and cH15/3 were produced using the baculovirus expression system as described in
616 detail previously (Margine et al., 2013). The ectodomains of the HA proteins were cloned
617 into a baculovirus shuttle vector. This shuttle vector contains a C-terminal trimerization
618 domain as well as a hexahistidine tag. Baculoviruses were propagated in Sf9 cells and
619 these viruses were then used to infect BTI-TN-5B1-4 cells. Proteins were purified from
620 the supernatant as described above.

621 Plasmids for expression of mAb 07-5G01 were generously contributed by Dr. Patrick
622 Wilson. The expression plasmids were transfected into Expi293F cells using an Expi293
623 transfection kit per the manufacturer's instructions. The supernatant was collected 7 days
624 post transfection and purified using CaptureSelect IgG-Fc (Multispecies) Affinity Matrix
625 (Thermo Scientific).

626

627 **Generation and selection of hybridomas secreting H15 antibodies**

628 Six to eight week-old female BALB/c mice were infected with a sublethal dose of A/wt
629 shearwater/WA/2576/1979 (H15N5) virus and boosted with an inactivated preparation of
630 the same virus. Three days after the boost, the mice were euthanized, and the spleens
631 were harvested. The splenocytes were fused with SP2/0 myeloma cells using
632 polyethylene glycol (PEG; Sigma-Aldrich) and the resultant fused cells were grown in
633 selection medium (Clonacell-HY Medium D; StemCell Technologies). Ten to fourteen days
634 later, individual colonies were picked and grown in 96-well plates. The supernatants from
635 these wells were screened via ELISA for binding to the A/wt shearwater/WA/2576/1979
636 HA. The clones which showed reactivity were isotyped using a Pierce rapid antibody
637 isotyping kit (Thermo scientific). The single clones were then further expanded using

638 Clonacell-HY Medium E (StemCell Technologies) and later adapted to serum free
639 medium (Hybridoma-SFM; Gibco). Once expanded to the desired volume, the
640 supernatants were collected, and the antibodies were purified using CaptureSelect IgG-
641 Fc (Multispecies) Affinity Matrix (Thermo Scientific).

642 All *in vivo* experiments were conducted in accordance with the guidelines of the Icahn
643 School of Medicine at Mount Sinai Institutional Animal Care and Use Committee (IACUC).

644

645 **ELISA**

646 96-well plates (Immulon-4 HBX, Thermo Scientific) were coated with 50 µl/well of
647 recombinant protein diluted to a concentration of 2 µg/ml in PBS and stored at 4°C
648 overnight. On the following day, the coating solution was discarded, and the plates were
649 blocked with 200 µl/well of 3% non-fat milk prepared in PBS with 0.1% Tween-20 (PBS-
650 T) for one hour at room temperature (RT). MAbs were diluted to a starting concentration
651 of 30 µg/ml and serially diluted 1:3 in 1% non-fat milk prepared in PBS-T. After one hour,
652 the blocking solution was discarded and 100 µl of the mAb dilutions were added to the
653 plates in duplicates and incubated for 2 hours at RT. The plates were then washed 3 times
654 with 200 µl/well of PBS-T. Next, 50 µl/well of the secondary antibodies [for mouse mAbs:
655 Sheep anti-mouse IgG (H&L) Antibody Peroxidase Conjugated antibody (Rockland
656 Immunochemicals), for human mAbs: Goat anti−human IgG (Fab-specific)−horseradish
657 peroxidase (HRP) labeled antibody (Sigma)] diluted to 1:3000 in 1% non-fat milk in PBS-
658 T was added and incubated at RT for 1 hour. The plates were washed 3 times with 200
659 µl/well of PBS-T. Following this, 100 µl/well of SigmaFAST OPD (o-phenylenediamine
660 dihydrochloride; Sigma-Aldrich) was added to the plates and incubated at RT for 10
661 minutes. The reaction was stopped by adding 50 µl/well of 3M hydrochloric acid (HCl;
662 Fisher Scientific) and analyzed at an optical density (OD) of 490 nm using SynergyH1
663 microplate reader (BioTek). For ELISA performed with purified virus, the purified virus was
664 coated on 96-well plates at concentration of 5 µg/ml in PBS and the protocol was followed
665 as described above.

666

667 **Immunofluorescence assay**

668 MDCK cells were seeded in a 96-well cell culture plate (Corning) at a density of 25,000
669 cells/well and cultured overnight at 37°C. The viruses were diluted in 1X minimum
670 essential medium (MEM). The cells were washed with 200 µl/well of PBS and infected
671 with a multiplicity of infection (MOI) of 1 for each respective virus at 37°C overnight. On
672 the following day, the cells were fixed with 100 µl/well of 3.7% paraformaldehyde for 1
673 hour at RT. Next, the wells were blocked with 200 µl/well of 3% non-fat milk prepared in
674 PBS for 1 hour at RT. After removing the blocking solution, 100 µl/well of each of the mAbs

675 diluted to 30 µg/ml in 1% non-fat milk prepared in PBS were added to the wells and
676 incubated at RT for 1 hour. After the incubation, the primary antibodies were removed,
677 and the cells were washed 3 times with PBS. 100 µl/well of secondary antibodies [for
678 mouse mAbs: Goat anti-Mouse IgG (H+L) Cross-Adsorbed Secondary Antibody, Alexa
679 Fluor 488 (Thermo Fisher Scientific), and for human mAbs: Goat anti-Human IgG (H+L)
680 Cross-Adsorbed Secondary Antibody, Alexa Fluor 488 (Thermo Fisher Scientific)] diluted
681 to 1 µg/ml and 4',6-diamidino-2-phenylindole, dilactate(DAPI; Thermo Scientific) diluted
682 to 1:500 in 1% non-fat milk in PBS were added to the wells and incubated at RT for 1 hour
683 covered in foil. The cells were washed 3 times with PBS and imaged using EVOS M5000
684 fluorescent imaging microscope (Thermo Scientific).

685

686 **Western blot assay**

687 Ten (10) ng of recombinant H15 from A/wt shearwater/WA/2576/1979 and H1 from
688 A/PR/8/34 (negative control) prepared in PBS were mixed with equal volume of 2x
689 Laemmli sample buffer supplemented with beta-mercaptoethanol and incubated at 95°C
690 for 20 minutes. The proteins were then loaded and run on 4-20% gradient SDS
691 polyacrylamide gel (Bio-Rad) and later transferred to nitrocellulose membranes using
692 iBlot 2 Gel Transfer Device (Invitrogen). The membranes were blocked with 3% non-fat
693 milk in PBS-T and later probed with 30 µg/ml of each mAb diluted in 1% non-fat milk in
694 PBS-T for 1 hour at RT. Anti-6x-His antibody (Thermo Fisher Scientific) was used as a
695 positive control. Following this, the membranes were washed 3 times with PBS-T and
696 stained with alkaline phosphatase (AP) conjugated secondary antibody (Sigma) for 1 hour
697 at RT. The blots were developed with AP conjugate substrate kit (Bio-Rad) according to
698 the manufacturer's protocol.

699

700 **Microneutralization assay**

701 MDCK cells were seeded in 96-well cell culture plates at a density of 25,000 cells/well
702 and cultured overnight at 37°C. The viruses were diluted to 100x 50% tissue culture
703 infectious dose ($TCID_{50}$)/50 µl and three-fold serial dilutions of mAbs starting at 30 µg/ml
704 in duplicates were prepared in 1X MEM supplemented with 1 µg/ml tosyl phenylalanyl
705 chloromethyl ketone (TPCK)-treated trypsin (Sigma). Antibody dilutions and viruses were
706 incubated together for 1 hour at RT on a shaking platform. The cells were washed with
707 PBS and the antibody-virus mix was added and incubated at 37°C for 1 hour. Another set
708 of mAb dilutions were prepared in 1X MEM supplemented with 1 µg/ml TPCK-treated
709 trypsin. At the end of the incubation, the cells were washed with PBS and mAb dilutions
710 prepared in 1X MEM with TPCK-treated trypsin were added. The cells were then
711 incubated at 37°C for 48 hours. At the end of the incubation, hemagglutination assays

712 were performed using the supernatant from infected cells and 0.5% chicken red blood
713 cells (RBCs; Lampire Biological Laboratories) diluted in PBS to test for the presence of
714 virus in each well.

715

716 **Hemagglutination inhibition assay (HI)**

717 MAbs were serially diluted 1:2 at a starting concentration of 30 µg/ml in PBS in v-bottom
718 96-well plates (Thermo Scientific). A hemagglutination assay was performed to determine
719 the hemagglutination titer (HAU) for the viruses. Twenty five µl of the mAb dilutions were
720 incubated with 25 µl of viruses diluted to 8 HAU for 1 hour at RT. Following this, 50 µl of
721 0.5% chicken RBCs diluted in PBS were added to the wells and incubated at 4°C for 1
722 hour and analyzed.

723 For the HI assay performed with mouse serum, sera were treated with receptor destroying
724 enzyme (RDE; Denka-Seiken) to remove non-specific inhibitors of hemagglutination.
725 Starting with an initial 1:10 dilution, the sera were serially diluted 1:2 in PBS in V-bottom
726 96-well plates. Twenty five µl of serum dilutions were incubated with 25 µl of viruses
727 diluted to 8 HAU for 1 hour at RT. Following this, 50 µl of 0.5% chicken RBCs diluted in
728 PBS was added to the wells and incubated at 4°C for 1 hour and analyzed.

729

730 **PRNA**

731 MDCK cells were seeded in 12-well cell culture plates (Corning) at a density of 250,000
732 cells/well and cultured overnight at 37°C. 1:5 serial dilutions of mAbs starting at 100 µg/ml
733 were prepared in 1X MEM and incubated with 1600 PFU/ml of A/wt
734 shearwater/WA/2576/1979 (H15N9) virus for 1 hour at RT with shaking. The virus-
735 antibody mixture was then transferred on MDCK cells in duplicates and incubated at 37°C
736 for 1 hour with intermittent shaking every 10 minutes to prevent drying out of cells.
737 Following the incubation, agar overlays containing corresponding mAb dilutions were
738 applied and the cells were incubated at 37°C for 48 hours. At the end of the 48 hours, the
739 cells were fixed using 3.7% paraformaldehyde for 1 hour at RT. The plates were blocked
740 with 3% non-fat milk in PBS. Plaques were stained using anti-H15 mouse polyclonal
741 serum diluted to 1:1000 in 1% non-fat milk in PBS for 1 hour at RT. Following PBS washes,
742 secondary antibody (sheep anti-mouse IgG (H&L)-Peroxidase Conjugated antibody;
743 Rockland Immunochemicals) diluted to 1:3000 in 1% non-fat milk in PBS was added to
744 the cells and incubated for 1 hour at RT. Cells were then washed again with PBS and 300
745 µl/well of TruBlue Peroxidase substrate (Seracare) was added to visualize and count the
746 plaques. Percent inhibition of number of plaques was calculated in comparison to a no-
747 antibody control, and the IC50, defined as the concentration of the mAb at which there

748 was a 50% reduction in number of plaques, was calculated on GraphPad Prism 10 using
749 a nonlinear regression model.

750

751 **ADCC reporter assay**

752 *In vitro* ADCC assay reporter kit (Promega) was used to determine the ADCC activity of
753 the mAbs. MDCK cells were seeded in 96-well white cell culture plates (Nunc) at a density
754 of 25,000 cells/well and cultured overnight at 37°C. The cells were infected with A/wt
755 shearwater/WA/2576/1979 (H15N9) virus at an MOI of 1 in 1x MEM and incubated
756 overnight at 37°C. 1:3 serial dilutions of mAbs at a starting concentration of 30 µg/ml were
757 prepared in Roswell Park Memorial Institute (RPMI)-1640 medium (Gibco). Following the
758 overnight incubation, the virus inoculum was removed from the cells. Twenty five µl of
759 RPMI-1640 medium supplemented with low IgG FBS (Gibco), 25 µl of antibody dilutions
760 and 25 µl of effector cells (75,000 cells/well) were added to each well and the plates were
761 incubated for 6 hours at 37°C. At the end of incubation, 75 µl of luciferase substrate was
762 added to each well and the plates were incubated for 10 minutes at RT covered in foil.
763 Following this, luminescence was captured as readout using the SynergyH1 microplate
764 reader.

765

766 **ELLA**

767 ELLAs were performed to assess the neuraminidase activity of the viruses. 96-well plates
768 (Immulon-4 HBX, Thermo Scientific) were coated with 100 µl/well of fetuin (Sigma) at a
769 concentration of 25 µg/ml in 1X coating buffer (Seracare) and stored at 4°C overnight.
770 The plates were incubated at 37°C with 2-fold serial dilutions of the viruses starting at a
771 1:10 initial dilution overnight. On the following day, the plates were washed 6 times with
772 PBS-T and were incubated with 100 µl/well of 5 µg/ml peanut agglutinin conjugated to
773 horseradish peroxidase (PNA-HRP; Sigma) for 2 hours at RT. Following this, the plates
774 were washed 3 times with PBS-T. Hundred µl/well of SigmaFAST OPD was added to the
775 plates and incubated at room temperature for 10 minutes. The reaction was stopped by
776 adding 50 µl/well of 3M HCl and analyzed at OD 490nm using SynergyH1 microplate
777 reader. The data was analyzed using GraphPad Prism 10 and 50% effective
778 concentration (EC_{50}) was determined for each virus.

779 To measure neuraminidase inhibition activity of the mAbs, the mAbs were serially diluted
780 1:3 at a starting concentration of 30 µg/ml and added to fetuin coated plates. An equal
781 volume of viruses diluted to $2xEC_{50}$ were added to the mAb dilutions and incubated at
782 37°C for 16-18 hours. The remainder of the assay was performed as described above.
783 Broadly reactive neuraminidase antibody 1G01 (Stadlbauer et al., 2019) or oseltamivir
784 phosphate (U.S. Pharmacopeia) was used as a positive control.

785

786 ***In vivo* mouse challenge studies**

787 Six to eight weeks old female BALB/c mice (n=5 per group) were injected with either 10
788 mg/kg, 2 mg/kg or 0.1 mg/kg of the mAbs intraperitoneally (IP). Two hours after
789 administration of mAbs, the mice were infected with 5 mLD50 of A/wt
790 shearwater/WA/2576/1979 (H15N5) intranasally (IN) under anesthesia and weights were
791 monitored daily for 14 days. Loss of 25% of body weight led to humane euthanasia and
792 the mouse was scored dead. The weight loss and survival curves were plotted using
793 GraphPad Prism 10.

794 To assess the effect of the mAbs on viral replication in the lungs of infected mice, 6-8
795 weeks old female BALB/c mice (n=6 per group) were injected with 10 mg/kg of the mAbs
796 IP. Two hours after administration of mAbs, the mice were infected with one mLD50 of
797 A/wt shearwater/WA/2576/1979 (H15N5) IN under anesthesia. 3 Three mice were
798 euthanized 3 DPI and their lungs were harvested. The remaining 3 mice in each group
799 were euthanized 6 DPI and their lungs were harvested. The lungs were homogenized
800 using BeadBlaster (Benchmark Scientific) and the supernatants were analyzed for viral
801 load using standard plaque assay.

802 To assess the serum HI responses elicited response to infection, 6-8 weeks old female
803 BALB/c mice (n=5 per group) were infected with 10^5 PFU (in 50 µl of PBS) of each of the
804 five H15 virus strains IN under anesthesia. Serum was collected at 21 DPI and tested in
805 an HAI assay against matched and heterologous H15 virus strains. Mice in the group
806 infected with A/wt shearwater/WA/2576/1979 (H15N9) virus were re-infected at 28 days
807 post initial infection and sera were collected 7 days post second infection for analysis in
808 HI assay.

809 All *in vivo* experiments were conducted in accordance with the guidelines of the Icahn
810 School of Medicine at Mount Sinai Institutional Animal Care and Use Committee (IACUC).

811

812 **Generation of escape mutant variants**

813 For mAbs with HI activity, 10^6 PFU of A/wt shearwater/WA/2576/1979 (H15N9) virus were
814 mixed with 250 µg of mAb and incubated at RT for 1 hour. Following the incubation, the
815 virus-mAb mixture was injected into 10-days old SPF embryonated chicken eggs (Charles
816 River Laboratories) and incubated at 37°C for 48 hours. The allantoic fluid was harvested
817 from the eggs at the end of incubation period and tested in HI assays for loss of HI activity.
818 The variants against which the corresponding mAbs showed complete lack of HI activity
819 were plaque purified on MDCK cells and grown in 10-days old SPF embryonated chicken
820 eggs. Alternatively, for neutralizing mAb without HI activity, A/wt

821 shearwater/WA/2576/1979 virus was incubated with 0.25xIC_{50} of mAb diluted in 1x MEM
822 supplemented with 1 µg/ml TPCK-treated trypsin at RT for 1 hour and used to infect
823 MDCK cells seeded in 12-well plates at 33°C for 72 hours. At the end of the incubation,
824 the supernatant was collected and a 1:10 dilution was incubated with 0.5xIC_{50} of mAb for
825 1 hour at RT and used to infect MDCK cells. The virus was serially passaged until
826 128xIC_{50} of mAb was reached. The supernatant from the final passage was used in an
827 immunofluorescence assay to confirm loss of binding. The variants were then plaque
828 purified on MDCK cells and grown in 10-days old SPF embryonated chicken eggs. RNA
829 was extracted from the allantoic fluid using E.Z.N.A. viral RNA extraction kit (Omega
830 Biotek) and cDNA was generated using the SuperScript III First Strand Synthesis System
831 (Invitrogen). HA segments were sequenced using Sanger sequencing to identify the
832 escape mutations. Wild type virus passaged in the presence of irrelevant mAb KL-H6-
833 8H9 was used as negative control to distinguish the escape mutations from other
834 mutations that may arise from adaptation to growth in cell culture or eggs.

835

836 **Sequencing variable regions of mAbs**

837 Variable regions of the murine mAbs were sequenced using Switching Mechanism At 5'
838 End of RNA Template (SMARTer 5') Rapid Amplification of cDNA Ends (RACE) kit (Takara
839 Bio). Total RNA from hybridoma cells was extracted using TRIzol reagent (Invitrogen).
840 cDNA was generated by reverse transcription using isotype specific constant gene 3'
841 primers, the SMARTer II A Oligonucleotide and SMARTScribe reverse transcriptase. The
842 cDNA was then amplified using SeqAmp DNA polymerase (Takara Bio) using a universal
843 5' primer mix and a nested 3' primer. The purified PCR products were Sanger sequenced
844 using the constant gene 3' primers and the obtained sequences were entered into the
845 international ImMunoGeneTics information system/V-QUERy and Standardization
846 (IMGT/V-QUEST) tool (https://www.imgt.org/IMGTindex/V-QUEST.php) to verify the
847 complete variable region sequence. For the cases with insufficient sequencing quality,
848 the PCR products were cloned into pRACE vector (Takara Bio) using In-Fusion Snap
849 Assembly mix (Takara Bio). The plasmids were amplified in Stellar competent cells
850 (Takara Bio) and miniprepped using QIAPrep Spin Miniprep Kit (Qiagen) prior to Sanger
851 sequencing and analysis using IMGT/V-QUEST. Sequences for 07-5G01 variable regions
852 were obtained from GenBank (heavy chain: KU987561.1, light chain: KU987562.1).

853

854 **IgG digestion**

855 Papain was activated by 15 min incubation at 37°C in a freshly prepared solution of 100
856 mM Tris, 2 mM EDTA, 10 mM L-cysteine, and 1 mg/ml papain. Purified monoclonal IgG
857 were digested at 37°C for 4-5 h with activated papain at a ratio of 40 µl activated papain

858 solution per mg of IgG to generate Fab. Iodoacetamide was added to a final concentration
859 of 0.03 M to halt digestion prior to concentration in a 10 kDa Amicon concentrator. Fab
860 was separated from Fc and undigested IgG by incubation with IgG Fc Capture Select
861 Multispecies (Thermo Fisher).

862

863 **Immune complexing and negative stain EM**

864 Fabs were incubated with A/wt shearwater/Western Australia/2576/1979 H15 HA at a 3:1
865 molar ratio for 1 hour at RT. Carbon-coated 400 mesh copper grids (Electron Microscopy
866 Services) were glow-discharged (PELCO easiGlow, Ted Pella Inc.) and 3 µl of immune
867 complexes were applied at a concentration of ~10-20 µg/ml. Excess sample was blotted
868 with Whatman filter paper and 3 µl of 2% w/v uranyl formate were applied to stain
869 complexes for 60 seconds (s) twice. Micrographs were collected using Leginon and were
870 imaged on a Tecnai F20 (FEI) with a TemCam F416 CMOS (Tietz Video and Image
871 Processing Systems GmbH) at 120 kV, 63,000 × magnification, and 1.67 Å/pixel (Suloway
872 et al., 2005). For each complex, 15k to 100k particles were picked and stacked using
873 Appion and subsequently processed using Relion 3.0 or Relion 4.0b1 (Kimanius et al.,
874 2021; Lander et al., 2009; Scheres, 2012; Suloway et al., 2005; Zivanov et al., 2018).
875 UCSF ChimeraX was used to generate composite 3D reconstructions (Pettersen et al.,
876 2021).

877

878 **CryoEM grid preparation**

879 For cryo-electron microcopy, A/wt shearwater/Western Australia/2576/1979 H15 was
880 functionalized with sulfo-NHS-SS-diazirine (Sulfo-SDAD) (Sigma Aldrich) using N-
881 hydroxysuccinimide (NHS)-ester chemistry as described previously and per commercial
882 protocols (Torrents de la Peña et al., 2023). Briefly, A/wt shearwater/Western
883 Australia/2576/1979 H15 in PBS was diluted to 1 mg/ml (~5.5 µM) and incubated with 40-
884 fold molar excess of freshly prepared Sulfo-SDAD solution in PBS for 30 minutes at RT.
885 To stop the NHS-ester reaction, 1M Tris-HCl, pH 8.0 was added to the solution at a final
886 concentration of 75 mM and the sample was incubated for 5 minutes at RT. Excess
887 crosslinker was removed using a 30 kDa Amicon concentrator.

888 To crosslink immune complexes, Fab were incubated with functionalized A/wt
889 shearwater/Western Australia/2576/1979 H15 for 30-60 minutes to facilitate binding and
890 the Sulfo-SDAD diazirine chemistry was subsequently activated by exposing the sample
891 to a ultraviolet (UV) dose of 1461.0 mJ/cm^2 using a UVP Crosslinker CL-3000 (Analytik
892 Jena). To minimize trimer degradation prior to freezing, A/wt shearwater/Western
893 Australia/2576/1979 H15 was stabilized by activating Sulfo-SDAD diazirine chemistry

894 prior to incubation with HL-H15-3G11 Fab. To improve tumbling, 07-5G01, KL-H15-6H4,
895 and KL-H15-6G8 were each separately co-incubated with CR9114 (Dreyfus et al., 2012)
896 Fab and A/wt shearwater/Western Australia/2576/1979 H15 prior to cross-linking at a
897 molar ratio of 3:3:1. KL-H15-6F6 Fab was co-incubated with CR9114 (Dreyfus et al.,
898 2012) Fab, and A/wt shearwater/Western Australia/2576/1979 H15 at a molar ratio of
899 3:3:3:1 prior to cross-linking.

900 Quantifoil R1.2/1.3 Cu, 300-mesh grids (Quantifoil Micro Tools GmbH) were plasma
901 treated with a PELCO easiGlow (Ted Pella Inc.) for 25 s at 15 mA immediately before use.
902 Grids were prepared using a Vitrobot Mark IV (Thermo Fisher Scientific) set to RT, blot
903 force 1, 100% humidity, wait time 5 s, and blot times between 3-6 s. Immune complexes
904 with final concentrations 0.65-0.75 mg/ml were mixed with n-octyl-beta-D-glucoside
905 (OBG) (Anatrace) to a final detergent concentration of 0.1% immediately before grid
906 application.

907

908 **Cryo-EM data collection**

909 The 07-5G01, KL-H15-6H4, and KL-H15-6G8 immune complexes were screened and
910 collected on a 300 kV Titan Krios (Thermo Fisher) equipped with a Bioquantum K3 direct
911 electron detector (Gatan). Automated data collection was conducted using Leginon at a
912 nominal magnification of 105,000×, a pixel size of 0.833 Å, an approximate exposure
913 dose of 50 e- /Å2 442, and a nominal defocus range of -0.8 to -1.5 µm (Suloway et al.,
914 2005). Data sets contained 2500-4500 micrographs. For each data collection, roughly
915 half of the micrographs were collected at 45° tilt to overcome orientation bias.

916 The KL-H15-3G11 and KL-H15-6F6 immune complexes were screened and collected on
917 a 200 kV Glacios (Thermo Fisher) equipped with a Falcon IV direct electron detector
918 (Thermo Fisher). For KL-H15-3G11, EPU (Thermo Fisher) was used for automated data
919 collection at 190,000× nominal magnification and a pixel size of 0.725 Å, with an
920 approximate exposure dose of 45 e- /Å2 442 and a nominal defocus range of -0.7 to -1.4
921 µm. Data for the 6F6 immune complex was collected using similar parameters, but on a
922 Glacios with a pixel size of 0.718. Data sets contained 3000-6500 micrographs each.

923

924 **Cryo-EM data processing**

925 For 07-5G01, KL-H15-6H4, and KL-H15-6G8, Appion was used for image preprocessing
926 and UCSF MotionCor2 was used for alignment and dose weighting (Lander et al., 2009).
927 For KL-H15-3G11 and KL-H15-6F6, CryoSPARC Live was used for image preprocessing
928 including alignment, motion correction, and CTF estimation (Punjani et al., 2017).

Initial processing for all immune complexes was done using CryoSPARC v3.0. A blob picker was used to pick initial particles for extraction. Following multiple rounds of 2D classification, clean particle stacks were used to generate templates for template picking. Following template picking and extraction, *Ab-Initio Reconstruction* was used to generate a starting map and to continue cleaning particle stacks. This was followed either by *Heterogeneous Refinement* if necessary to improve initial resolution and alignment or a *Homogenous Refinement* if the initial *Ab-Initio Reconstruction* was already homogenous and well-aligned. For KL-H15-6H4 and KL-H15-3G11, subsequent rounds of *Homogenous Refinement* and *Non-uniform Refinement* were sufficient to generate maps of sufficient quality for model building. For 07-5G01, the *Topaz* neural network pipeline was used to improve particle picking (Bepler et al., 2019). Briefly, intensive *2D Classification* and *Rebalance 2D* were used to generate the highest quality templates for *Topaz Training*. *Topaz Extract* was used to pick high-quality particles which were subsequently extracted for use in an *Ab-Initio Reconstruction* followed by iterative rounds of *Heterogeneous*, *Homogenous*, and finally *Non-uniform Refinements*. For KL-H15-6F6 and KL-H15-6G8, particles from a *Non-uniform Refinement* job resulting from a similar processing pathway as KL-H15-6H4 and KL-H15-3G11 were transferred to Relion 4.01b (Kimanius et al., 2021). These particles were further processed using Relion 4.01b *3D Autorefine* and *CTF Refinement* before undergoing C3 symmetry expansion and focused *3D Classification* to isolate bound H15 HA protomers. Bound particles were used for a final round of *3D Autorefine* and *Post-processing* to generate final maps for model building. Final maps were deposited to the EMDB with accession codes found in Table S1.

Atomic model building

A crystal structure of A/wt shearwater/Western Australia/2576/1979 H15 HA (PDB: 5TG8) was used as a starting model for the trimer and ABodyBuilder 2.0 was used to generate starting models of 07-5G01, KL-H15-6H4, KL-H15-3G11, KL-H15-6G8, and KL-H15-6F6 (Abanades et al., 2023; Tzarum et al., 2017). Initial models of trimer and Fab were rigid body docked into the corresponding EM maps in ChimeraX and manually refined using Coot (Emsley & Cowtan, 2004). Iterations of Phenix real-space refinement and manual refinement in Coot were used to improve model statistics (Liebschner et al., 2019). Map-to-model fit was validated using Molprobity and EMRinger in Phenix (Barad et al., 2015; Chen et al., 2010). Final models were deposited to the PDB with accession codes found in Table S1. Figures containing maps and/or EM models were generated using ChimeraX. All H15 models are in H15 numbering, and all Fabs are deposited using the Kabat numbering scheme.

967 **Phylogenetic analysis**

968 Amino acid sequences of the respective HA proteins were obtained from GenBank.
969 Alignment of the sequences was performed using Clustal Omega and the phylogenetic
970 tree was built using the neighbor-joining tree method. The tree was finally visualized and
971 labeled using Figtree v1.4.4.4.

972

973 **Quantification and statistical analysis**

974 Statistical analysis was performed using GraphPad Prism 10 using non-linear regression
975 for Figure 2 and 3, and survival analysis was visualized using Kaplan-Meier curves for
976 Figure 4.

977

978 **SUPPLEMENTAL FIGURE TITLES AND LEGENDS**

979 **Figure S1**: Binding and HI activity of mAbs. (A) Binding of mAbs to purified A/wt
980 shearwater/WA/2576/1979 virus assessed by ELISA. The broadly cross-reactive HA
981 antibody CR9114 (Dreyfus et al., 2012) was used as a positive control and anti-H6
982 antibody KL-H6-8H9 was used as negative control. (B) Binding to A/wt
983 shearwater/WA/2576/1979 recombinant H15 in Western blot following a reducing
984 denaturing SDS-PAGE. A/PR8/34 H1 was used to test for nonspecific binding, and an
985 anti-hexahistidine antibody was used as a positive control. (C) HI activity of mAbs
986 measured against panel of H15 viruses from 2008 to 2015. Minimal concentration at
987 which HI activity was observed is shown here. Anti-H6 antibody KL-H6-8H9 was used as
988 negative control.

989 **Figure S2**: Plaque size reduction, NAI and ADCC activity of mAbs. (A) Reduction in
990 plaque size observed in PRNA with A/wt shearwater/WA/2576/1979. Shown here are the
991 plaques observed in the well treated with the lowest measured concentration of mAb KL-
992 H15-6H4 as a representative of the treatment with neutralizing mAbs. The plaques
993 observed in wells treated with anti-H6 antibody KL-H6-8H9 used as negative control are
994 shown for comparison. (B) NAI activity of mAbs measured against panel of H15 viruses
995 from 2008 to 2015 measured by ELLA. Broadly cross-reactive influenza virus
996 neuraminidase antibody 1G01 (Stadlbauer et al., 2019) was used as a positive control,
997 while anti-H6 antibody KL-H6-8H9 was used as negative control. Neuraminidase inhibitor
998 oseltamivir was used as a positive control for NAI against A/mallard
999 duck/Sweden/139647/2012 virus. (C) ADCC activity of mAbs was measured using
1000 antigen-specific ADCC reporter assay (Promega) using both mouse and human ADCC
1001 effector cells and the area under the curve (AUC) values are shown here. The broadly

cross-reactive HA antibody CR9114 (Dreyfus et al., 2012) was used as a positive control and anti-H6 antibody KL-H6-8H9 was used as negative control.

Figure S3: Negative stain EM maps of KL-H15-6G8, -3G11, and –6F6 Fabs complexed with A/wt shearwater/WA/2576/1979 H15 HA. Segmented Fabs from Relion 3.0 reconstructions were colored by mAb and displayed on a negative stain map of A/Hong Kong/4801/2014 H3 as a representative Group 2 HA. Representative 2D class averages of particles used to generate reconstructions are displayed below the corresponding map.

Figure S4: ClustalW multiple sequence alignment of heavy-chain and light-chain complementarity determining regions (CDRs) for all five mAbs reveal conserved regions within and across mAb classes. Residues are colored by conservation of side chain chemistry using ClustalW conventions.

Figure S5: CryoEM maps, Fourier shell correlation (FSC) plots, representative 2D classes, and representative micrographs for mAb complexes. All five maps presented sequentially in rows A-E, colored by local resolution. FSC maps generated in Relion 4.01b (A and E) or CryoSPARC v4 (B-D) with resolutions reported to coincide with gold-standard FSC cutoff 0.143. All 2D classes were generated in cryoSPARC v4.

Figure S6: Map, footprint, and complementarity determining region usage for KL-H15-6F6 mAb. (A) Final KL-H15-6F6 EM map colored by proximity to A/wt shearwater/WA/2576/1979 H15 HA and KL-H15-6F6 Fv docked into density using ChimeraX. Light-chain depicted in light orange and heavy-chain depicted in burnt orange. (B) KL-H15-6F6 footprint on surface depiction of A/wt shearwater/WA/2576/1979 H15 HA. (C) CDRs involved in antigen engagement as demonstrated by EM map and GetContacts program (https://getcontacts.github.io/index.html, Table S2).

REFERENCES:

Abanades, B., Wong, W. K., Boyles, F., Georges, G., Bujotzek, A., & Deane, C. M. (2023). ImmuneBuilder: Deep-Learning models for predicting the structures of immune proteins. *Commun Biol*, *6*(1), 575. https://doi.org/10.1038/s42003-023-04927-7

Bahl, K., Senn, J. J., Yuzhakov, O., Bulychev, A., Brito, L. A., Hassett, K. J., Laska, M. E., Smith, M., Almarsson, Ö., Thompson, J., Ribeiro, A. M., Watson, M., Zaks, T., & Ciaramella, G. (2017). Preclinical and Clinical Demonstration of Immunogenicity by mRNA Vaccines against H10N8 and H7N9 Influenza Viruses. *Mol Ther*, *25*(6), 1316-1327. https://doi.org/10.1016/j.ymthe.2017.03.035

Banyard, A. C., Bennison, A., Byrne, A. M. P., Reid, S. M., Lynton-Jenkins, J. G., Mollett, B., De Silva, D., Peers-Dent, J., Finlayson, K., Hall, R., Blockley, F., Blyth, M., Falchieri, M., Fowler, Z., Fitzcharles, E. M., Brown, I. H., & James, J. (2024). Detection and spread of high pathogenicity avian influenza virus H5N1 in the

Antarctic Region. *Nature Communications*, *15*(1), 7433. https://doi.org/10.1038/s41467-024-51490-8

Barad, B. A., Echols, N., Wang, R. Y., Cheng, Y., DiMaio, F., Adams, P. D., & Fraser, J. S. (2015). EMRinger: side chain-directed model and map validation for 3D cryo-electron microscopy. *Nat Methods*, *12*(10), 943-946. https://doi.org/10.1038/nmeth.3541

Beare, A. S., Schild, G. C., & Craig, J. W. (1975). Trials in man with live recombinants made from A/PR/8/34 (H0 N1) and wild H3 N2 influenza viruses. *Lancet*, *2*(7938), 729-732. https://doi.org/10.1016/s0140-6736(75)90720-5

Bepler, T., Morin, A., Rapp, M., Brasch, J., Shapiro, L., Noble, A. J., & Berger, B. (2019). Positive-unlabeled convolutional neural networks for particle picking in cryo-electron micrographs. *Nat Methods*, *16*(11), 1153-1160. https://doi.org/10.1038/s41592-019-0575-8

Boon, A. C., Sandbulte, M. R., Seiler, P., Webby, R. J., Songserm, T., Guan, Y., & Webster, R. G. (2007). Role of terrestrial wild birds in ecology of influenza A virus (H5N1). *Emerg Infect Dis*, *13*(11), 1720-1724. https://doi.org/10.3201/eid1311.070114

Brandenburg, B., Koudstaal, W., Goudsmit, J., Klaren, V., Tang, C., Bujny, M. V., Korse, H. J. W. M., Kwaks, T., Otterstrom, J. J., Juraszek, J., van Oijen, A. M., Vogels, R., & Friesen, R. H. E. (2013). Mechanisms of hemagglutinin targeted influenza virus neutralization. *PLoS One*, *8*(12), e80034. Retrieved 2013, from http://europepmc.org/abstract/MED/24348996

https://journals.plos.org/plosone/article/file?id=10.1371/journal.pone.0080034&type=printable

https://doi.org/10.1371/journal.pone.0080034

https://europepmc.org/articles/PMC3862845

https://europepmc.org/articles/PMC3862845?pdf=render

Carey, C. (2009). The impacts of climate change on the annual cycles of birds. *Philos Trans R Soc Lond B Biol Sci*, *364*(1534), 3321-3330. https://doi.org/10.1098/rstb.2009.0182

Causey, D., & Edwards, S. V. (2008). Ecology of avian influenza virus in birds. *J Infect Dis*, *197 Suppl 1*(Suppl 1), S29-33. https://doi.org/10.1086/524991

Chen, C.-J., Ermler, M. E., Tan, G. S., Krammer, F., Palese, P., & Hai, R. (2016). Influenza A Viruses Expressing Intra- or Intergroup Chimeric Hemagglutinins. *Journal of Virology*, *90*(7), 3789-3793. https://doi.org/doi:10.1128/jvi.03060-15

Chen, L., & Khanna, M. (2024). Heterogeneous and long-term effects of a changing climate on bird biodiversity. *Global Environmental Change Advances*, *2*, 100008. https://doi.org/https://doi.org/10.1016/j.gecadv.2024.100008

Chen, V. B., Arendall, W. B., 3rd, Headd, J. J., Keedy, D. A., Immormino, R. M., Kapral, G. J., Murray, L. W., Richardson, J. S., & Richardson, D. C. (2010). MolProbity: all-atom structure validation for macromolecular crystallography. *Acta Crystallogr D Biol Crystallogr*, *66*(Pt 1), 12-21. https://doi.org/10.1107/s0907444909042073

Claas, E. C., Osterhaus, A. D., van Beek, R., De Jong, J. C., Rimmelzwaan, G. F., Senne, D. A., Krauss, S., Shortridge, K. F., & Webster, R. G. (1998). Human influenza A

1082 H5N1 virus related to a highly pathogenic avian influenza virus. *Lancet*, *351*(9101),
1083 472-477. https://doi.org/10.1016/s0140-6736(97)11212-0
1084 Dascalu, S., Sealy, J. E., Sadeyen, J. R., Flammer, P. G., Fiddaman, S., Preston, S. G.,
1085 Dixon, R. J., Bonsall, M. B., Smith, A. L., & Iqbal, M. (2024). Immunisation of
1086 chickens with inactivated and/or infectious H9N2 avian influenza virus leads to
1087 differential immune B-cell repertoire development. *Front Immunol*, *15*, 1461678.
1088 https://doi.org/10.3389/fimmu.2024.1461678
1089 Dezfuli, A., Horton, K. G., Zuckerberg, B., Schubert, S. D., & Bosilovich, M. G. (2022).
1090 Continental Patterns of Bird Migration Linked to Climate Variability. *Bulletin of the*
1091 *American Meteorological Society*, *103*(2), E536-E547.
1092 https://doi.org/https://doi.org/10.1175/BAMS-D-21-0220.1
1093 Dreyfus, C., Laursen, N. S., Kwaks, T., Zuijdgeest, D., Khayat, R., Ekiert, D. C., Lee, J.
1094 H., Metlagel, Z., Bujny, M. V., Jongeneelen, M., van der Vlugt, R., Lamrani, M.,
1095 Korse, H. J. W. M., Geelen, E., Sahin, Ö., Sieuwerts, M., Brakenhoff, J. P. J.,
1096 Vogels, R., Li, O. T. W.,…Friesen, R. H. E. (2012). Highly Conserved Protective
1097 Epitopes on Influenza B Viruses. *Science*, *337*(6100), 1343-1348.
1098 https://doi.org/doi:10.1126/science.1222908
1099 El-Shesheny, R., Feeroz, M. M., Krauss, S., Vogel, P., McKenzie, P., Webby, R. J., &
1100 Webster, R. G. (2018). Replication and pathogenic potential of influenza A virus
1101 subtypes H3, H7, and H15 from free-range ducks in Bangladesh in mammals.
1102 *Emerg Microbes Infect*, *7*(1), 70. https://doi.org/10.1038/s41426-018-0072-7
1103 Emsley, P., & Cowtan, K. (2004). Coot: model-building tools for molecular graphics. *Acta*
1104 *Crystallogr D Biol Crystallogr*, *60*(Pt 12 Pt 1), 2126-2132.
1105 https://doi.org/10.1107/s0907444904019158
1106 Fadlallah, G. M., Ma, F., Zhang, Z., Hao, M., Hu, J., Li, M., Liu, H., Liang, B., Yao, Y.,
1107 Gong, R., Zhang, B., Liu, D., & Chen, J. (2020). Vaccination with Consensus H7
1108 Elicits Broadly Reactive and Protective Antibodies against Eurasian and North
1109 American Lineage H7 Viruses. *Vaccines (Basel)*, *8*(1).
1110 https://doi.org/10.3390/vaccines8010143
1111 Gao, R., Cao, B., Hu, Y., Feng, Z., Wang, D., Hu, W., Chen, J., Jie, Z., Qiu, H., Xu, K., Xu,
1112 X., Lu, H., Zhu, W., Gao, Z., Xiang, N., Shen, Y., He, Z., Gu, Y., Zhang, Z.,…Shu,
1113 Y. (2013). Human infection with a novel avian-origin influenza A (H7N9) virus. *N*
1114 *Engl J Med*, *368*(20), 1888-1897. https://doi.org/10.1056/NEJMoa1304459
1115 Gilchuk, I. M., Bangaru, S., Kose, N., Bombardi, R. G., Trivette, A., Li, S., Turner, H. L.,
1116 Carnahan, R. H., Ward, A. B., & Crowe, J. E., Jr. (2021). Human antibody
1117 recognition of H7N9 influenza virus HA following natural infection. *JCI Insight*,
1118 *6*(19). https://doi.org/10.1172/jci.insight.152403
1119 Hanmer, H. J., Cunningham, A. A., John, S. K., Magregor, S. K., Robinson, R. A., Seilern-
1120 Moy, K., Siriwardena, G. M., & Lawson, B. (2022). Hinfluences severe disease-
1121 mediated population declines in two of the most common garden bird species in
1122 Great Britain. *Sci Rep*, *12*(1), 15055. https://doi.org/10.1038/s41598-022-18880-8
1123 Hassan, M. M., El Zowalaty, M. E., Islam, A., Khan, S. A., Rahman, M. K., Järhult, J. D.,
1124 & Hoque, M. A. (2020). Prevalence and Diversity of Avian Influenza Virus
1125 Hemagglutinin Sero-Subtypes in Poultry and Wild Birds in Bangladesh. *Vet Sci*,
1126 *7*(2). https://doi.org/10.3390/vetsci7020073

1127 Henry Dunand, C. J., Leon, P. E., Huang, M., Choi, A., Chromikova, V., Ho, I. Y., Tan, G.
1128 S., Cruz, J., Hirsh, A., Zheng, N. Y., Mullarkey, C. E., Ennis, F. A., Terajima, M.,
1129 Treanor, J. J., Topham, D. J., Subbarao, K., Palese, P., Krammer, F., & Wilson, P.
1130 C. (2016). Both Neutralizing and Non-Neutralizing Human H7N9 Influenza
1131 Vaccine-Induced Monoclonal Antibodies Confer Protection. *Cell Host Microbe*,
1132 *19*(6), 800-813. https://doi.org/10.1016/j.chom.2016.05.014
1133 Hill, S. C., Manvell, R. J., Schulenburg, B., Shell, W., Wikramaratna, P. S., Perrins, C.,
1134 Sheldon, B. C., Brown, I. H., & Pybus, O. G. (2016). Antibody responses to avian
1135 influenza viruses in wild birds broaden with age. *Proc Biol Sci*, *283*(1845).
1136 https://doi.org/10.1098/rspb.2016.2159
1137 Horton, K. G., Buler, J. J., Anderson, S. J., Burt, C. S., Collins, A. C., Dokter, A. M., Guo,
1138 F., Sheldon, D., Tomaszewska, M. A., & Henebry, G. M. (2023). Artificial light at
1139 night is a top predictor of bird migration stopover density. *Nat Commun*, *14*(1),
1140 7446. https://doi.org/10.1038/s41467-023-43046-z
1141 Huang, Y., Li, X., Zhang, H., Chen, B., Jiang, Y., Yang, L., Zhu, W., Hu, S., Zhou, S., Tang,
1142 Y., Xiang, X., Li, F., Li, W., & Gao, L. (2015). Human infection with an avian
1143 influenza A (H9N2) virus in the middle region of China. *Journal of Medical Virology*,
1144 *87*(10), 1641-1648. https://doi.org/https://doi.org/10.1002/jmv.24231
1145 Kamal, R. P., Blanchfield, K., Belser, J. A., Music, N., Tzeng, W. P., Holiday, C., Burroughs,
1146 A., Sun, X., Maines, T. R., Levine, M. Z., & York, I. A. (2017). Inactivated H7
1147 Influenza Virus Vaccines Protect Mice despite Inducing Only Low Levels of
1148 Neutralizing Antibodies. *J Virol*, *91*(20). https://doi.org/10.1128/jvi.01202-17
1149 Karakus, U., Mena, I., Kottur, J., El Zahed, S. S., Seoane, R., Yildiz, S., Chen, L.,
1150 Plancarte, M., Lindsay, L., Halpin, R., Stockwell, T. B., Wentworth, D. E., Boons,
1151 G. J., Krammer, F., Stertz, S., Boyce, W., de Vries, R. P., Aggarwal, A. K., & García-
1152 Sastre, A. (2024). H19 influenza A virus exhibits species-specific MHC class II
1153 receptor usage. *Cell Host Microbe*, *32*(7), 1089-1102.e1010.
1154 https://doi.org/10.1016/j.chom.2024.05.018
1155 Katzner, T., Blackford, A., Donahue, M., Gibbs, S. E. J., Lenoch, J., Martin, M., Rocke, T.,
1156 Root, J. J., Styles, D., Cooper, S., Dean, K., Dvornicky-Raymond, Z., Keller, D.,
1157 Sanchez, C., Dunlap, B., Grier, T., Jones, M., Nitzel, G., Patrick, E.,…Suarez, D.
1158 (2025). Safety and Immunogenicity of Poultry Vaccine for Protecting Critically
1159 Endangered Avian Species against Highly Pathogenic Avian Influenza Virus,
1160 United States. *Emerging Infectious Disease journal*, *31*(6), 1131.
1161 https://doi.org/10.3201/eid3106.241558
1162 Kayali, G., Barbour, E., Dbaibo, G., Tabet, C., Saade, M., Shaib, H. A., Debeauchamp, J.,
1163 & Webby, R. J. (2011). Evidence of infection with H4 and H11 avian influenza
1164 viruses among Lebanese chicken growers. *PLoS One*, *6*(10), e26818.
1165 https://doi.org/10.1371/journal.pone.0026818
1166 Khare, S., Gurry, C., Freitas, L., Schultz, M. B., Bach, G., Diallo, A., Akite, N., Ho, J., Lee,
1167 R. T., Yeo, W., Curation Team, G. C., & Maurer-Stroh, S. (2021). GISAID's Role in
1168 Pandemic Response. *China CDC Wkly*, *3*(49), 1049-1051.
1169 https://doi.org/10.46234/ccdcw2021.255
1170 Kimanius, D., Dong, L., Sharov, G., Nakane, T., & Scheres, S. H. W. (2021). New tools
1171 for automated cryo-EM single-particle analysis in RELION-4.0. *Biochem J*,
1172 *478*(24), 4169-4185. https://doi.org/10.1042/bcj20210708

1173 Kleyheeg, E., Slaterus, R., Bodewes, R., Rijks, J. M., Spierenburg, M. A. H., Beerens, N.,
1174 Kelder, L., Poen, M. J., Stegeman, J. A., Fouchier, R. A. M., Kuiken, T., & van der
1175 Jeugd, H. P. (2017). Deaths among Wild Birds during Highly Pathogenic Avian
1176 Influenza A(H5N8) Virus Outbreak, the Netherlands. *Emerg Infect Dis*, *23*(12),
1177 2050-2054. https://doi.org/10.3201/eid2312.171086
1178 Krammer, F., Smith, G. J. D., Fouchier, R. A. M., Peiris, M., Kedzierska, K., Doherty, P.
1179 C., Palese, P., Shaw, M. L., Treanor, J., Webster, R. G., & García-Sastre, A. (2018).
1180 Influenza. *Nat Rev Dis Primers*, *4*(1), 3. https://doi.org/10.1038/s41572-018-0002-
1181 y
1182 Lander, G. C., Stagg, S. M., Voss, N. R., Cheng, A., Fellmann, D., Pulokas, J., Yoshioka,
1183 C., Irving, C., Mulder, A., Lau, P. W., Lyumkis, D., Potter, C. S., & Carragher, B.
1184 (2009). Appion: an integrated, database-driven pipeline to facilitate EM image
1185 processing. *J Struct Biol*, *166*(1), 95-102. https://doi.org/10.1016/j.jsb.2009.01.002
1186 Leslie, G. A., & Clem, L. W. (1969). Phylogen of immunoglobulin structure and function.
1187 3. Immunoglobulins of the chicken. *J Exp Med*, *130*(6), 1337-1352.
1188 https://doi.org/10.1084/jem.130.6.1337
1189 Li, M., Chen, L., Wang, Q., Hao, M., Zhang, X., Liu, L., Yu, X., Yang, C., Xu, J., Chen, J.,
1190 & Gong, R. (2019). A cross-reactive human monoclonal antibody targets the
1191 conserved H7 antigenic site A from fifth wave H7N9-infected humans. *Antiviral*
1192 *Res*, *170*, 104556. https://doi.org/10.1016/j.antiviral.2019.104556
1193 Liebschner, D., Afonine, P. V., Baker, M. L., Bunkóczi, G., Chen, V. B., Croll, T. I., Hintze,
1194 B., Hung, L. W., Jain, S., McCoy, A. J., Moriarty, N. W., Oeffner, R. D., Poon, B. K.,
1195 Prisant, M. G., Read, R. J., Richardson, J. S., Richardson, D. C., Sammito, M. D.,
1196 Sobolev, O. V.,…Adams, P. D. (2019). Macromolecular structure determination
1197 using X-rays, neutrons and electrons: recent developments in Phenix. *Acta*
1198 *Crystallogr D Struct Biol*, *75*(Pt 10), 861-877.
1199 https://doi.org/10.1107/s2059798319011471
1200 Margine, I., Palese, P., & Krammer, F. (2013). Expression of functional recombinant
1201 hemagglutinin and neuraminidase proteins from the novel H7N9 influenza virus
1202 using the baculovirus expression system. *J Vis Exp*(81), e51112.
1203 https://doi.org/10.3791/51112
1204 Martínez-Sobrido, L., & García-Sastre, A. (2010). Generation of recombinant influenza
1205 virus from plasmid DNA. *J Vis Exp*(42). https://doi.org/10.3791/2057
1206 Meade, P., Latorre-Margalef, N., Stallknecht, D. E., & Krammer, F. (2017). Development
1207 of an influenza virus protein microarray to measure the humoral response to
1208 influenza virus infection in mallards. *Emerg Microbes Infect*, *6*(12), e110.
1209 https://doi.org/10.1038/emi.2017.98
1210 Muzyka, D., Pantin-Jackwood, M., Spackman, E., Stegniy, B., Rula, O., & Shutchenko, P.
1211 (2012). Avian influenza virus wild bird surveillance in the Azov and Black Sea
1212 regions of Ukraine (2010-2011). *Avian Dis*, *56*(4 Suppl), 1010-1016.
1213 https://doi.org/10.1637/10157-040912-ResNote.1
1214 Nachbagauer, R., Choi, A., Hirsh, A., Margine, I., Iida, S., Barrera, A., Ferres, M., Albrecht,
1215 R. A., García-Sastre, A., Bouvier, N. M., Ito, K., Medina, R. A., Palese, P., &
1216 Krammer, F. (2017). Defining the antibody cross-reactome directed against the
1217 influenza virus surface glycoproteins. *Nat Immunol*, *18*(4), 464-473.
1218 https://doi.org/10.1038/ni.3684

1219 Pettersen, E. F., Goddard, T. D., Huang, C. C., Meng, E. C., Couch, G. S., Croll, T. I.,
1220 Morris, J. H., & Ferrin, T. E. (2021). UCSF ChimeraX: Structure visualization for
1221 researchers, educators, and developers. *Protein Sci*, *30*(1), 70-82.
1222 https://doi.org/10.1002/pro.3943
1223 Popova, L., Smith, K., West, A. H., Wilson, P. C., James, J. A., Thompson, L. F., & Air, G.
1224 M. (2012). Immunodominance of antigenic site B over site A of hemagglutinin of
1225 recent H3N2 influenza viruses. *PLoS One*, *7*(7), e41895.
1226 https://doi.org/10.1371/journal.pone.0041895
1227 Punjani, A., Rubinstein, J. L., Fleet, D. J., & Brubaker, M. A. (2017). cryoSPARC:
1228 algorithms for rapid unsupervised cryo-EM structure determination. *Nat Methods*,
1229 *14*(3), 290-296. https://doi.org/10.1038/nmeth.4169
1230 Qi, L., Pujanauski, L. M., Davis, A. S., Schwartzman, L. M., Chertow, D. S., Baxter, D.,
1231 Scherler, K., Hartshorn, K. L., Slemons, R. D., Walters, K. A., Kash, J. C., &
1232 Taubenberger, J. K. (2014). Contemporary avian influenza A virus subtype H1, H6,
1233 H7, H10, and H15 hemagglutinin genes encode a mammalian virulence factor
1234 similar to the 1918 pandemic virus H1 hemagglutinin. *mBio*, *5*(6), e02116.
1235 https://doi.org/10.1128/mBio.02116-14
1236 Rajendran, M., Nachbagauer, R., Ermler, M. E., Bunduc, P., Amanat, F., Izikson, R., Cox,
1237 M., Palese, P., Eichelberger, M., & Krammer, F. (2017). Analysis of Anti-Influenza
1238 Virus Neuraminidase Antibodies in Children, Adults, and the Elderly by ELISA and
1239 Enzyme Inhibition: Evidence for Original Antigenic Sin. *mBio*, *8*(2),
1240 10.1128/mbio.02281-02216. https://doi.org/doi:10.1128/mbio.02281-16
1241 Röhm, C., Zhou, N., Süss, J., Mackenzie, J., & Webster, R. G. (1996). Characterization
1242 of a novel influenza hemagglutinin, H15: criteria for determination of influenza A
1243 subtypes. *Virology*, *217*(2), 508-516. https://doi.org/10.1006/viro.1996.0145
1244 Sano, K., Saito, S., Suzuki, T., Kotani, O., Ainai, A., van Riet, E., Tabata, K., Saito, K.,
1245 Takahashi, Y., Yokoyama, M., Sato, H., Maruno, T., Usami, K., Uchiyama, S.,
1246 Ogawa-Goto, K., & Hasegawa, H. (2021). An influenza HA stalk reactive polymeric
1247 IgA antibody exhibits anti-viral function regulated by binary interaction between HA
1248 and the antibody. *PLoS One*, *16*(1), e0245244.
1249 https://doi.org/10.1371/journal.pone.0245244
1250 Scheres, S. H. (2012). RELION: implementation of a Bayesian approach to cryo-EM
1251 structure determination. *J Struct Biol*, *180*(3), 519-530.
1252 https://doi.org/10.1016/j.jsb.2012.09.006
1253 Sehgal, R. N. (2010). Deforestation and avian infectious diseases. *J Exp Biol*, *213*(6),
1254 955-960. https://doi.org/10.1242/jeb.037663
1255 Shi, W., Shi, Y., Wu, Y., Liu, D., & Gao, G. F. (2013). Origin and molecular characterization
1256 of the human-infecting H6N1 influenza virus in Taiwan. *Protein Cell*, *4*(11), 846-
1257 853. https://doi.org/10.1007/s13238-013-3083-0
1258 Shipley, J. R., Twining, C. W., Mathieu-Resuge, M., Parmar, T. P., Kainz, M., Martin-
1259 Creuzburg, D., Weber, C., Winkler, D. W., Graham, C. H., & Matthews, B. (2022).
1260 Climate change shifts the timing of nutritional flux from aquatic insects. *Curr Biol*,
1261 *32*(6), 1342-1349.e1343. https://doi.org/10.1016/j.cub.2022.01.057
1262 Sivay, M. V., Baranovich, T., Marchenko, V. Y., Sharshov, K. A., Govorkova, E. A.,
1263 Shestopalov, A. M., & Webby, R. J. (2013). Influenza A (H15N4) virus isolation in

Western Siberia, Russia. *J Virol*, *87*(6), 3578-3582. https://doi.org/10.1128/JVI.02521-12

Spackman, E. (2009). The ecology of avian influenza virus in wild birds: what does this mean for poultry? *Poult Sci*, *88*(4), 847-850. https://doi.org/10.3382/ps.2008-00336

Stadlbauer, D., Zhu, X., McMahon, M., Turner, J. S., Wohlbold, T. J., Schmitz, A. J., Strohmeier, S., Yu, W., Nachbagauer, R., Mudd, P. A., Wilson, I. A., Ellebedy, A. H., & Krammer, F. (2019). Broadly protective human antibodies that target the active site of influenza virus neuraminidase. *Science*, *366*(6464), 499-504. https://doi.org/10.1126/science.aay0678

Suloway, C., Pulokas, J., Fellmann, D., Cheng, A., Guerra, F., Quispe, J., Stagg, S., Potter, C. S., & Carragher, B. (2005). Automated molecular microscopy: the new Leginon system. *J Struct Biol*, *151*(1), 41-60. https://doi.org/10.1016/j.jsb.2005.03.010

To, K. K. W., Tsang, A. K. L., Chan, J. F. W., Cheng, V. C. C., Chen, H., & Yuen, K.-Y. (2014). Emergence in China of human disease due to avian influenza A(H10N8) – Cause for concern? *Journal of Infection*, *68*(3), 205-215. https://doi.org/10.1016/j.jinf.2013.12.014

Torrents de la Peña, A., Sewall, L. M., de Paiva Froes Rocha, R., Jackson, A. M., Pratap, P. P., Bangaru, S., Cottrell, C. A., Mohanty, S., Shaw, A. C., & Ward, A. B. (2023). Increasing sensitivity of antibody-antigen interactions using photo-cross-linking. *Cell Rep Methods*, *3*(6), 100509. https://doi.org/10.1016/j.crmeth.2023.100509

Tzarum, N., McBride, R., Nycholat, C. M., Peng, W., Paulson, J. C., & Wilson, I. A. (2017). Unique Structural Features of Influenza Virus H15 Hemagglutinin. *J Virol*, *91*(12). https://doi.org/10.1128/JVI.00046-17

Vandegrift, K. J., Sokolow, S. H., Daszak, P., & Kilpatrick, A. M. (2010). Ecology of avian influenza viruses in a changing world. *Ann N Y Acad Sci*, *1195*, 113-128. https://doi.org/10.1111/j.1749-6632.2010.05451.x

Wang, X., Chen, Y., Melville, D. S., Choi, C.-Y., Tan, K., Liu, J., Li, J., Zhang, S., Cao, L., & Ma, Z. (2022). Impacts of habitat loss on migratory shorebird populations and communities at stopover sites in the Yellow Sea. *Biological Conservation*, *269*, 109547. https://doi.org/https://doi.org/10.1016/j.biocon.2022.109547

Wohlbold, T. J., Chromikova, V., Tan, G. S., Meade, P., Amanat, F., Comella, P., Hirsh, A., & Krammer, F. (2016). Hemagglutinin Stalk- and Neuraminidase-Specific Monoclonal Antibodies Protect against Lethal H10N8 Influenza Virus Infection in Mice. *J Virol*, *90*(2), 851-861. https://doi.org/10.1128/jvi.02275-15

Wu, N. C., Otwinowski, J., Thompson, A. J., Nycholat, C. M., Nourmohammad, A., & Wilson, I. A. (2020). Major antigenic site B of human influenza H3N2 viruses has an evolving local fitness landscape. *Nat Commun*, *11*(1), 1233. https://doi.org/10.1038/s41467-020-15102-5

Yang, H., Carney, P. J., Chang, J. C., & Stevens, J. (2020). Molecular characterization and three-dimensional structures of avian H8, H11, H14, H15 and swine H4 influenza virus hemagglutinins. *Heliyon*, *6*(6), e04068. https://doi.org/https://doi.org/10.1016/j.heliyon.2020.e04068

Yuen, K. Y., Chan, P. K., Peiris, M., Tsang, D. N., Que, T. L., Shortridge, K. F., Cheung, P. T., To, W. K., Ho, E. T., Sung, R., & Cheng, A. F. (1998). Clinical features and rapid

1310 viral diagnosis of human disease associated with avian influenza A H5N1 virus.
1311 *Lancet*, *351*(9101), 467-471. https://doi.org/10.1016/s0140-6736(98)01182-9
1312 Zhang, X., Calvert, R. A., Sutton, B. J., & Doré, K. A. (2017). IgY: a key isotype in antibody
1313 evolution. *Biol Rev Camb Philos Soc*, *92*(4), 2144-2156.
1314 https://doi.org/10.1111/brv.12325
1315 Zimova, M., Willard, D. E., Winger, B. M., & Weeks, B. C. (2021). Widespread shifts in
1316 bird migration phenology are decoupled from parallel shifts in morphology. *J Anim*
1317 *Ecol*, *90*(10), 2348-2361. https://doi.org/10.1111/1365-2656.13543
1318 Zivanov, J., Nakane, T., Forsberg, B. O., Kimanius, D., Hagen, W. J., Lindahl, E., &
1319 Scheres, S. H. (2018). New tools for automated high-resolution cryo-EM structure
1320 determination in RELION-3. *Elife*, *7*. https://doi.org/10.7554/eLife.42166

1321

A

B

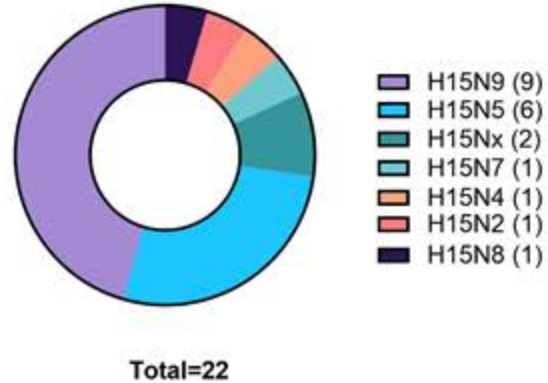

C

Monoclonal Antibody	Origin
KL-H15-3G11	Mouse Hybridoma
KL-H15-6F6	Mouse Hybridoma
KL-H15-6G8	Mouse Hybridoma
KL-H15-6H4	Mouse Hybridoma
07-5G01	Human

D

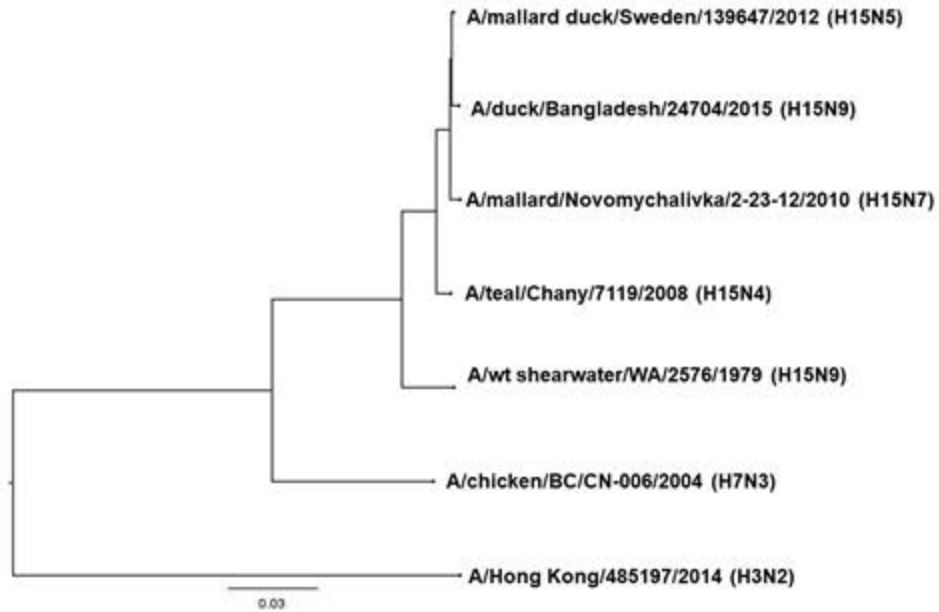

E

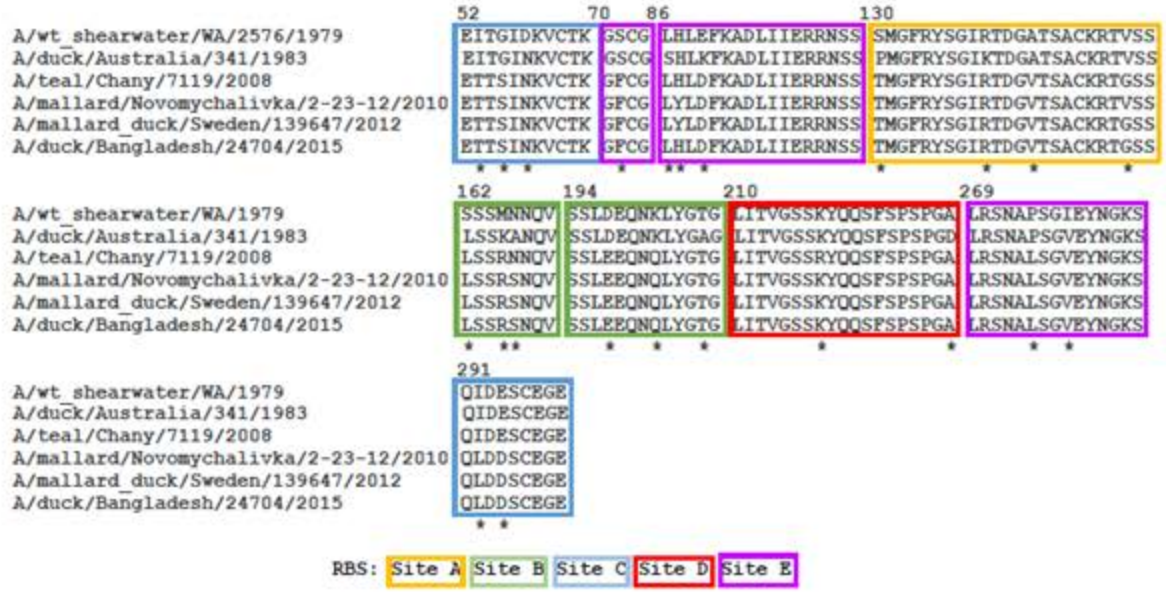

A

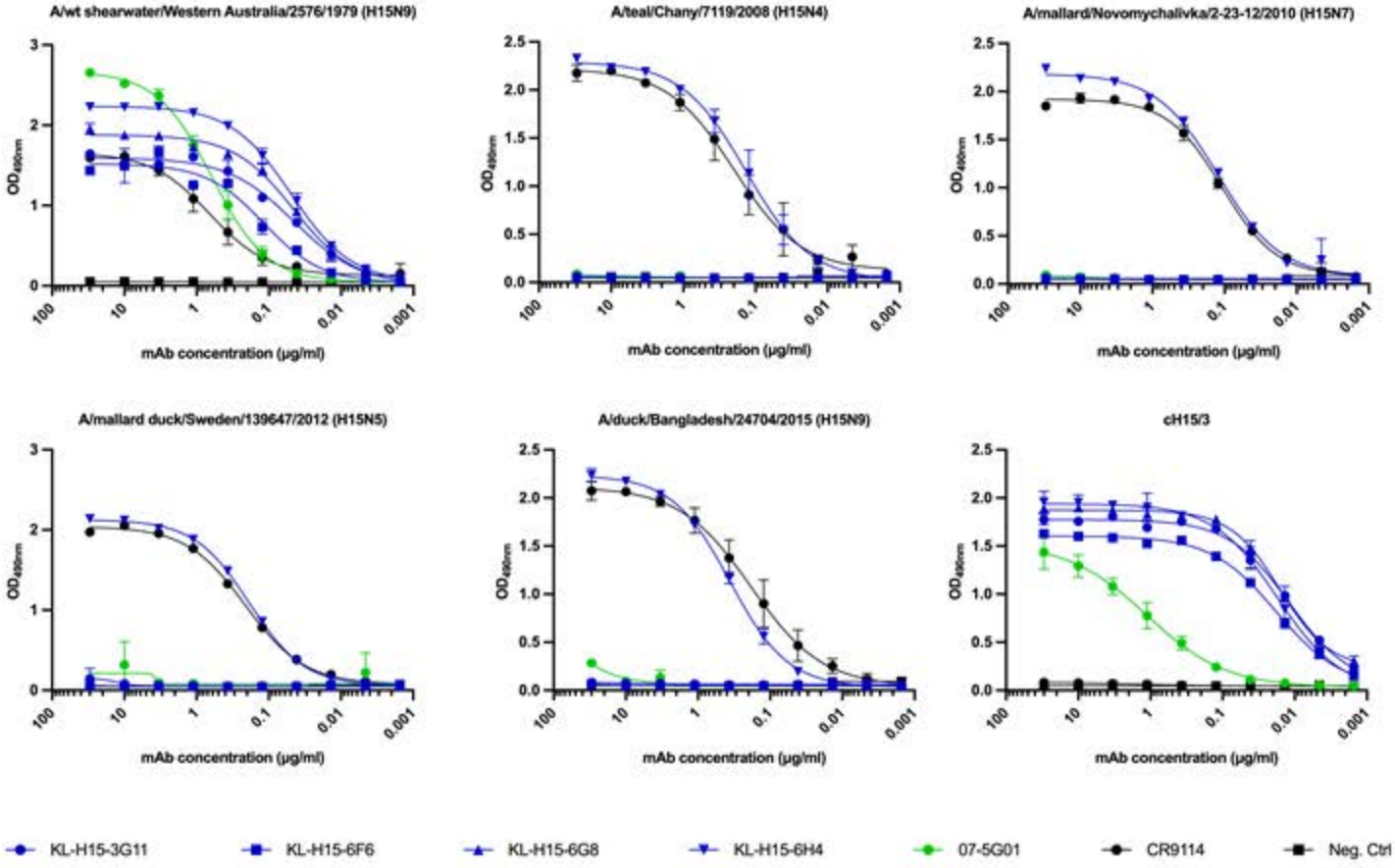
A/wt shearwater/Western Australia/2576/1979 (H15N9)
A/teal/Chany/7119/2008 (H15N4)
A/mallard/Novomychalivka/2-23-12/2010 (H15N7)
A/mallard duck/Sweden/139647/2012 (H15N5)
A/duck/Bangladesh/24704/2015 (H15N9)
cH15/3
OD450nm
mAb concentration (µg/ml)
KL-H15-3G11
KL-H15-6F6
KL-H15-6G8
KL-H15-6H4
07-5G01
CR9114
Neg. Ctrl

B

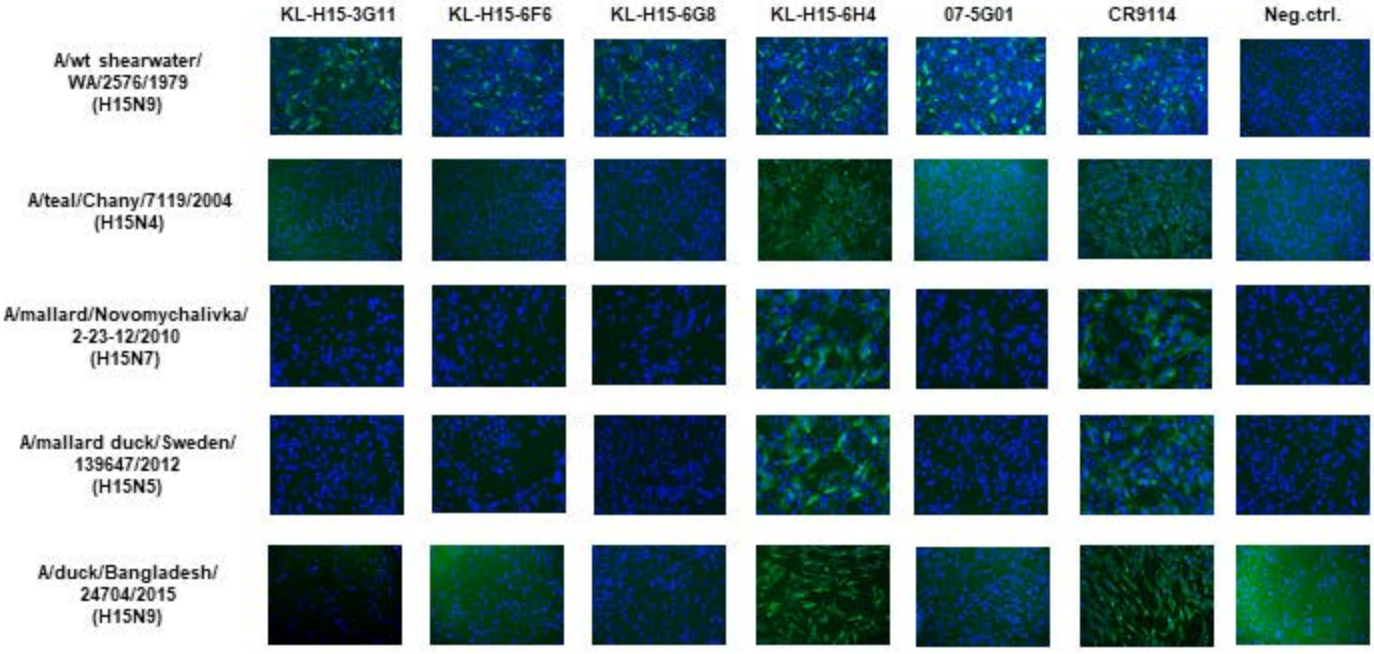
KL-H15-3G11
KL-H15-6F6
KL-H15-6G8
KL-H15-6H4
07-5G01
CR9114
Neg.ctrl.
A/wt shearwater/ WA/2576/1979 (H15N9)
A/teal/Chany/7119/2004 (H15N4)
A/mallard/Novomychalivka/ 2-23-12/2010 (H15N7)
A/mallard duck/Sweden/ 139647/2012 (H15N5)
A/duck/Bangladesh/ 24704/2015 (H15N9)

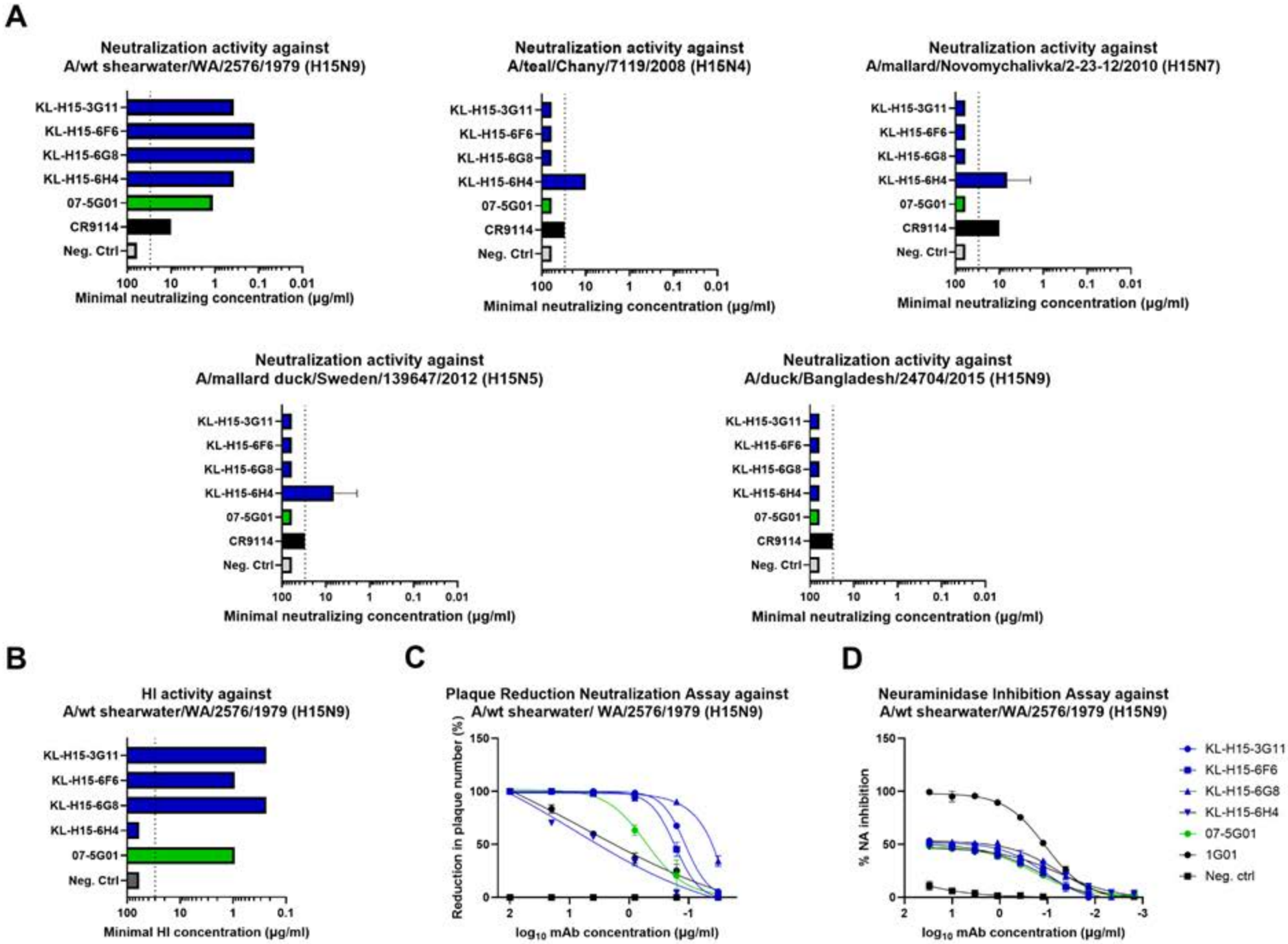
A
Neutralization activity against
A/wt shearwater/WA/2576/1979 (H15N9)
Neutralization activity against
A/teal/Chany/7119/2008 (H15N4)
Neutralization activity against
A/mallard/Novomychalivka/2-23-12/2010 (H15N7)
Neutralization activity against
A/mallard duck/Sweden/139647/2012 (H15N5)
Neutralization activity against
A/duck/Bangladesh/24704/2015 (H15N9)
KL-H15-3G11
KL-H15-6F6
KL-H15-6G8
KL-H15-6H4
07-5G01
CR9114
Neg. Ctrl
100
10
1
0.1
0.01
Minimal neutralizing concentration (µg/ml)
B
HI activity against
A/wt shearwater/WA/2576/1979 (H15N9)
Minimal HI concentration (µg/ml)
C
Plaque Reduction Neutralization Assay against
A/wt shearwater/ WA/2576/1979 (H15N9)
Reduction in plaque number (%)
log10 mAb concentration (µg/ml)
D
Neuraminidase Inhibition Assay against
A/wt shearwater/WA/2576/1979 (H15N9)
% NA inhibition
log10 mAb concentration (µg/ml)
KL-H15-3G11
KL-H15-6F6
KL-H15-6G8
KL-H15-6H4
07-5G01
1G01
Neg. ctrl

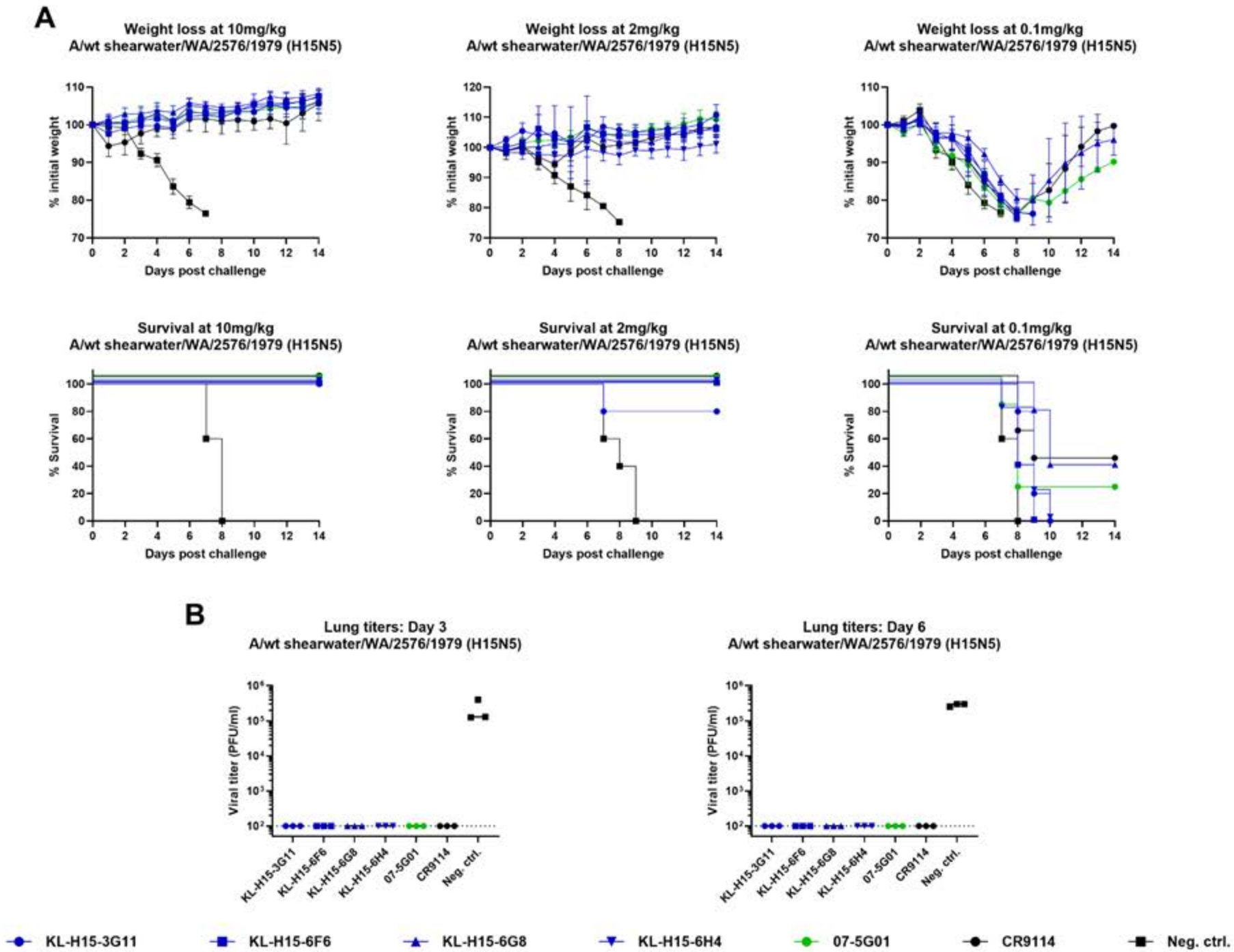
A
Weight loss at 10mg/kg
A/wt shearwater/WA/2576/1979 (H15N5)
Weight loss at 2mg/kg
A/wt shearwater/WA/2576/1979 (H15N5)
Weight loss at 0.1mg/kg
A/wt shearwater/WA/2576/1979 (H15N5)
% initial weight
Days post challenge
Survival at 10mg/kg
A/wt shearwater/WA/2576/1979 (H15N5)
Survival at 2mg/kg
A/wt shearwater/WA/2576/1979 (H15N5)
Survival at 0.1mg/kg
A/wt shearwater/WA/2576/1979 (H15N5)
% Survival
Days post challenge
B
Lung titers: Day 3
A/wt shearwater/WA/2576/1979 (H15N5)
Lung titers: Day 6
A/wt shearwater/WA/2576/1979 (H15N5)
Viral titer (PFU/ml)
KL-H15-3G11
KL-H15-6F6
KL-H15-6G8
KL-H15-6H4
07-5G01
CR9114
Neg. ctrl.

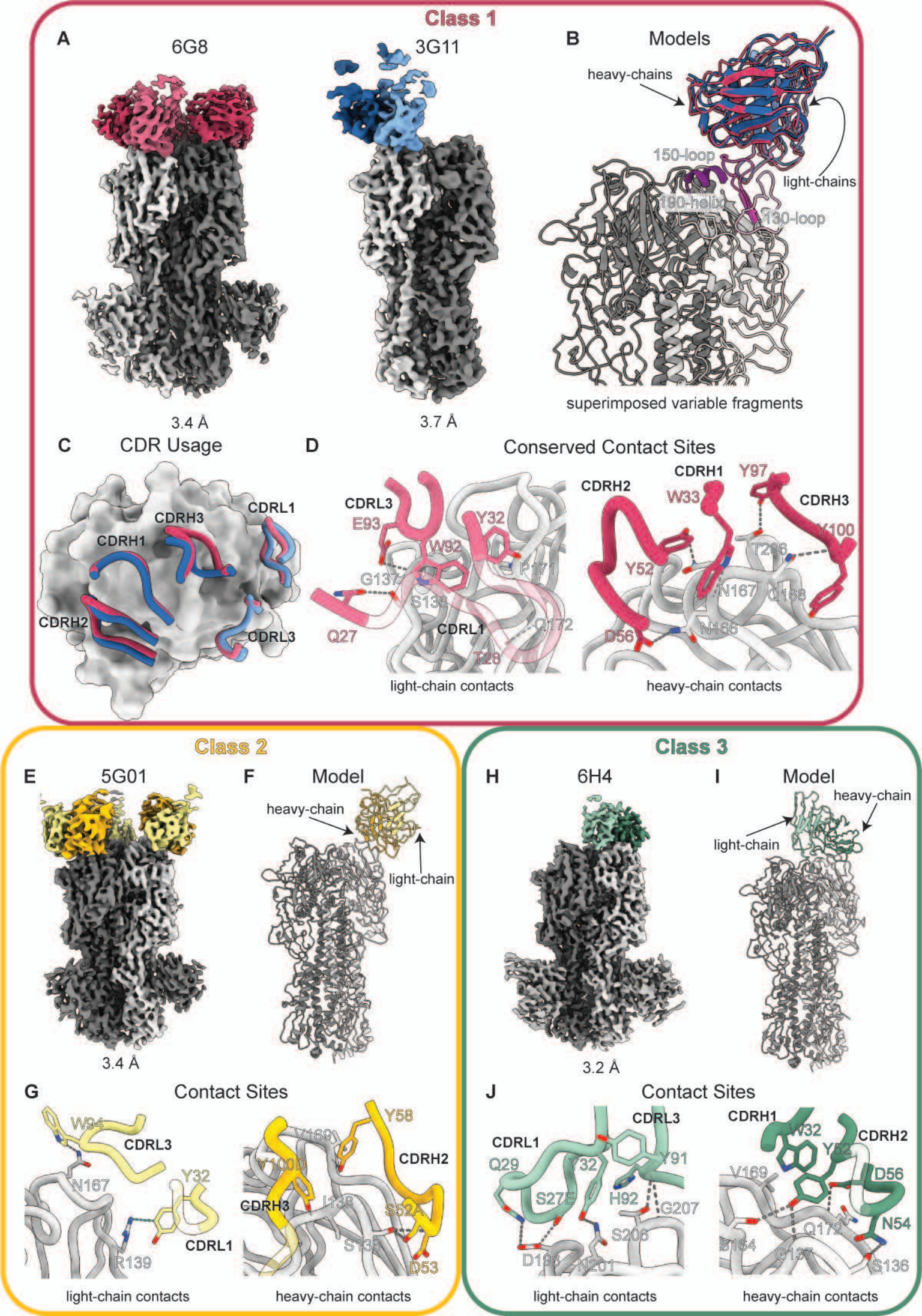
Class 1
A
6G8
3G11
3.4 Å
3.7 Å
B
Models
heavy-chains
150-loop
light-chains
180-helix
130-loop
superimposed variable fragments
C
CDR Usage
CDRH3
CDRL1
CDRH1
CDRH2
CDRL3
D
Conserved Contact Sites
CDRL3
E93
Y32
W92
P171
G137
S138
Q27
CDRL1
Q172
T28
light-chain contacts
CDRH2
CDRH1
Y97
W33
CDRH3
Y100
T206
Y52
N167
Q168
D56
N166
heavy-chain contacts
Class 2
E
5G01
3.4 Å
F
Model
heavy-chain
light-chain
G
Contact Sites
W94
CDRL3
N167
Y32
R139
CDRL1
light-chain contacts
Y58
V169
CDRH2
Y100D
CDRH3
I138
S52A
S135
D53
heavy-chain contacts
Class 3
H
6H4
3.2 Å
I
Model
heavy-chain
light-chain
J
Contact Sites
CDRL3
CDRL1
Q29
Y32
Y91
S27E
H92
G207
S206
D198
N201
light-chain contacts
CDRH1
W32
CDRH2
Y52
V169
D56
N54
Q172
S164
G137
S136
heavy-chain contacts

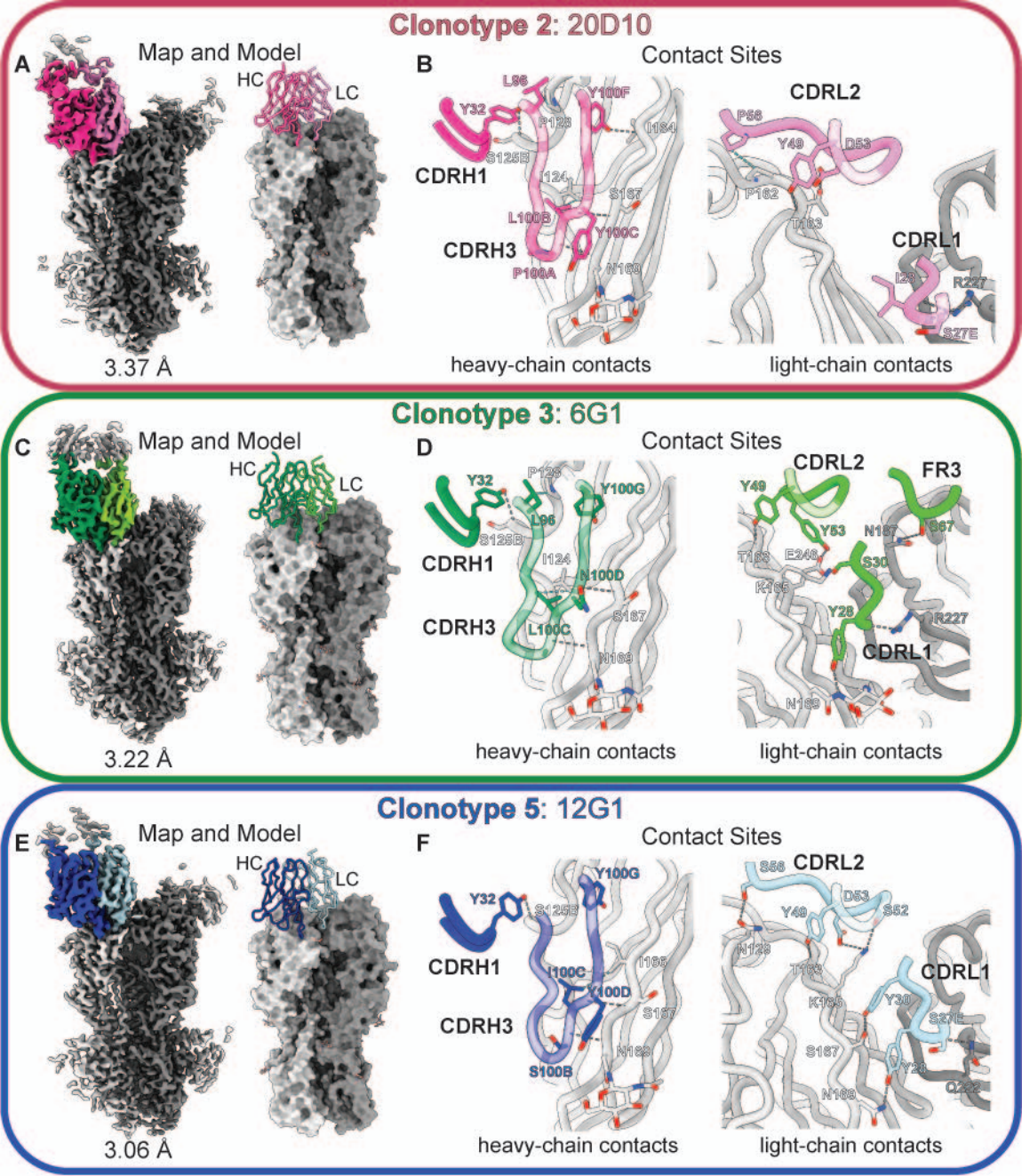
Clonotype 2: 20D10
A
Map and Model
HC
LC
3.37 Å
B
Contact Sites
L96
Y32
Y100F
P128
I184
S125B
CDRH1
I124
S187
L100B
Y100C
CDRH3
P100A
N189
heavy-chain contacts
CDRL2
P58
Y49
D53
P162
T163
CDRL1
I28
R227
S27E
light-chain contacts
Clonotype 3: 6G1
C
Map and Model
HC
LC
3.22 Å
D
Contact Sites
Y32
P128
Y100G
L96
S125B
CDRH1
I124
N100D
S187
CDRH3
L100C
N189
heavy-chain contacts
CDRL2
FR3
Y49
Y53
N187
S67
T163
E248
S30
K166
Y28
R227
CDRL1
N189
light-chain contacts
Clonotype 5: 12G1
E
Map and Model
HC
LC
3.06 Å
F
Contact Sites
Y100G
Y32
S125B
CDRH1
I100C
I166
Y100D
S187
CDRH3
N189
S100B
heavy-chain contacts
S58
CDRL2
D53
Y49
S52
N189
T163
CDRL1
K166
Y30
S27E
S187
Y28
Q222
N189
light-chain contacts

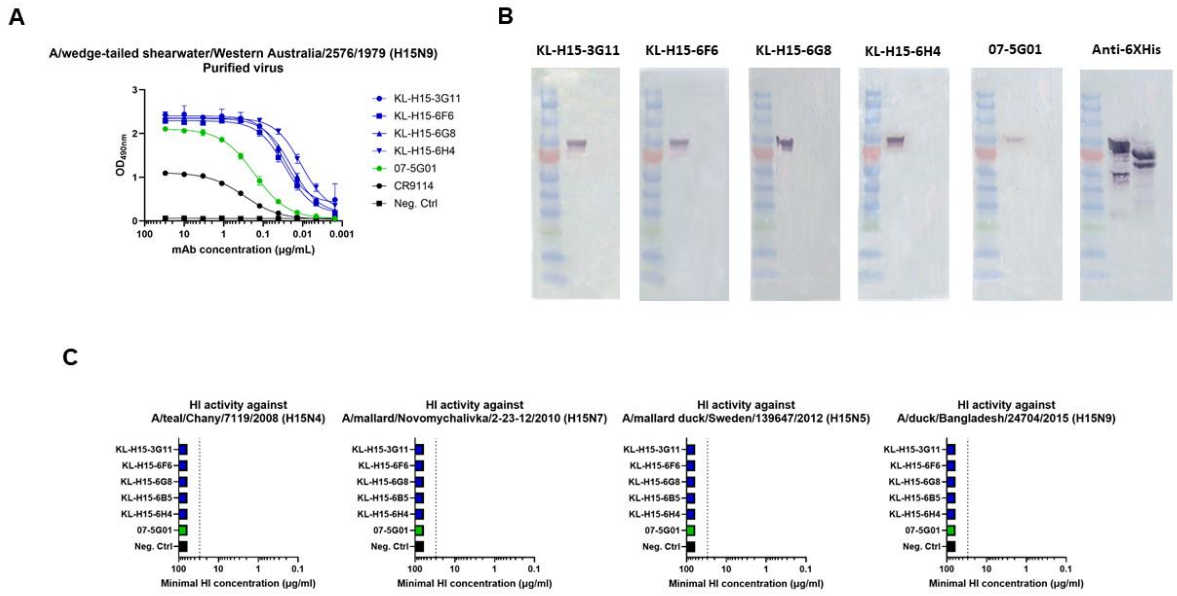

Figure S1: Binding and HI activity of mAbs. (A) Binding of mAbs to purified A/wt shearwater/WA/2576/1979 virus assessed by ELISA. The broadly cross-reactive HA antibody CR9114 (Dreyfus et al., 2012) was used as a positive control and anti-H6 antibody KL-H6-8H9 was used as negative control. (B) Binding to A/wt shearwater/WA/2576/1979 recombinant H15 in Western blot following a reducing denaturing SDS-PAGE. A/PR8/34 H1 was used to test for nonspecific binding, and an anti-hexahistidine antibody was used as a positive control. (C) HI activity of mAbs measured against panel of H15 viruses from 2008 to 2015. Minimal concentration at which HI activity was observed is shown here. Anti-H6 antibody KL-H6-8H9 was used as negative control.

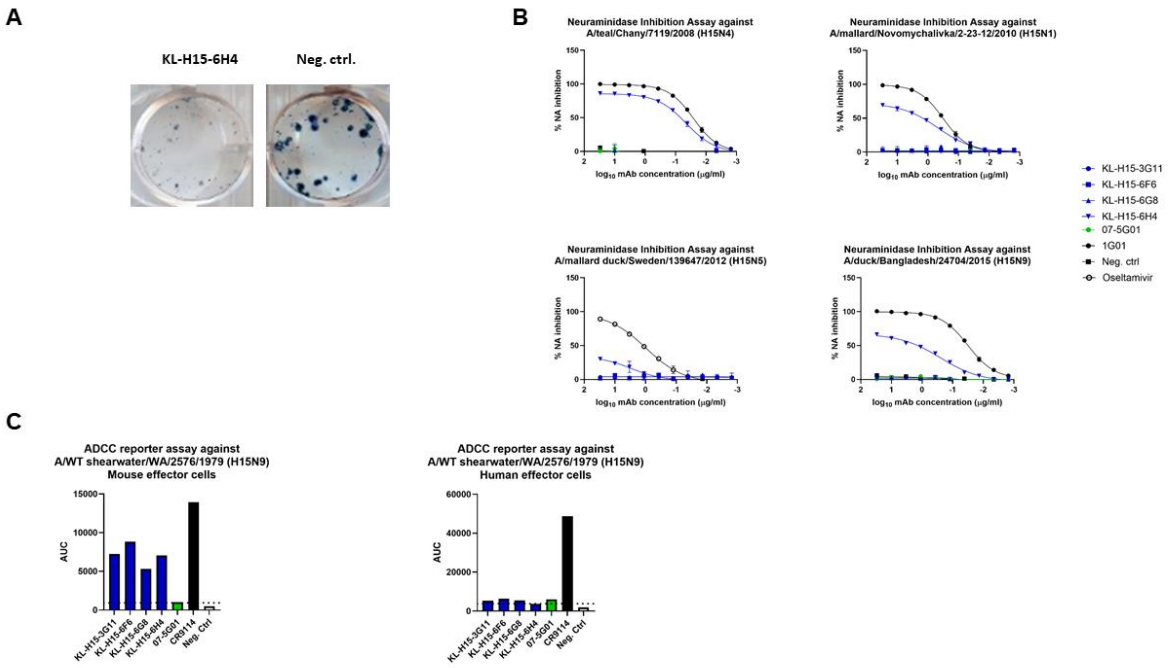

Figure S2: Plaque size reduction, NAI and ADCC activity of mAbs. (A) Reduction in plaque size observed in PRNA with A/wt shearwater/WA/2576/1979. Shown here are the plaques observed in the well treated with the lowest measured concentration of mAb KL-H15-6H4 as a representative of the treatment with neutralizing mAbs. The plaques observed in wells treated with anti-H6 antibody KL-H6-8H9 used as negative control are shown for comparison. (B) NAI activity of mAbs measured against panel of H15 viruses from 2008 to 2015 measured by ELLA. Broadly cross-reactive influenza virus neuraminidase antibody 1G01 (Stadlbauer et al., 2019) was used as a positive control, while anti-H6 antibody KL-H6-8H9 was used as negative control. Neuraminidase inhibitor oseltamivir was used as a positive control for NAI against A/mallard duck/Sweden/139647/2012 virus. (C) ADCC activity of mAbs was measured using antigen-specific ADCC reporter assay (Promega) using both mouse and human ADCC effector cells and the area under the curve (AUC) values are shown here. The broadly cross-reactive HA antibody CR9114 (Dreyfus et al., 2012) was used as a positive control and anti-H6 antibody KL-H6-8H9 was used as negative control.

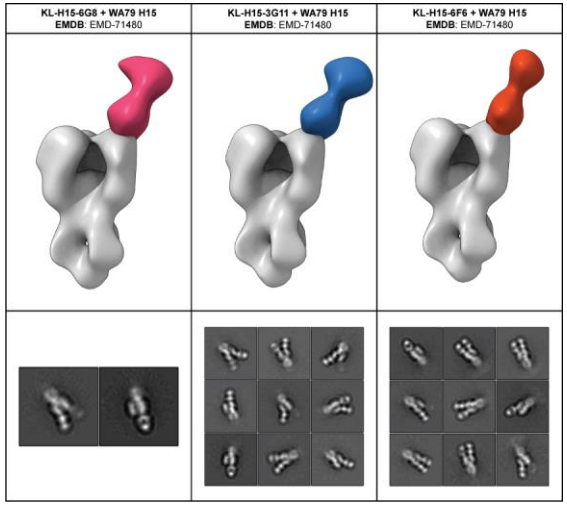

Figure S3: Negative stain EM maps of KL-H15-6G8, -3G11, and –6F6 Fabs complexed with A/wt shearwater/WA/2576/1979 H15 HA. Segmented Fabs from Relion 3.0 reconstructions were colored by mAb and displayed on a negative stain map of A/Hong Kong/4801/2014 H3 as a representative Group 2 HA. Representative 2D class averages of particles used to generate reconstructions are displayed below the corresponding map.

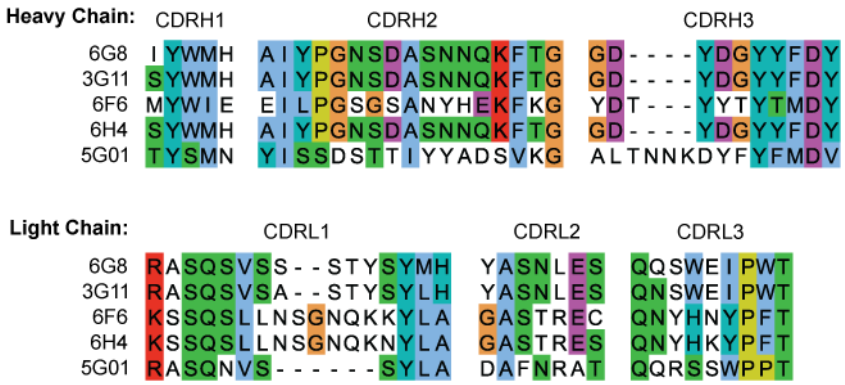

Figure S4: ClustalW multiple sequence alignment of heavy-chain and light-chain complementarity determining regions (CDRs) for all five mAbs reveal conserved regions within and across mAb classes. Residues are colored by conservation of side chain chemistry using ClustalW conventions.

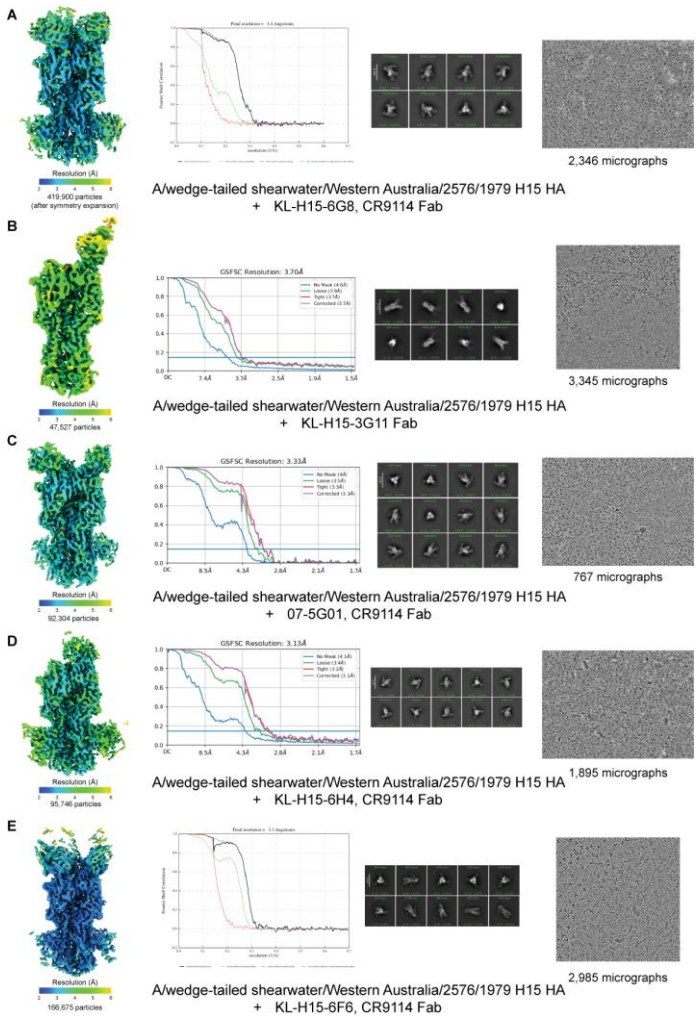

Figure S5: CryoEM maps, Fourier shell correlation (FSC) plots, representative 2D classes, and representative micrographs for mAb complexes. All five maps presented sequentially in rows A-E, colored by local resolution. FSC maps generated in Relion 4.01b (A and E) or CryoSPARC v4 (B-D) with resolutions reported to coincide with gold-standard FSC cutoff 0.143. All 2D classes were generated in cryoSPARC v4.

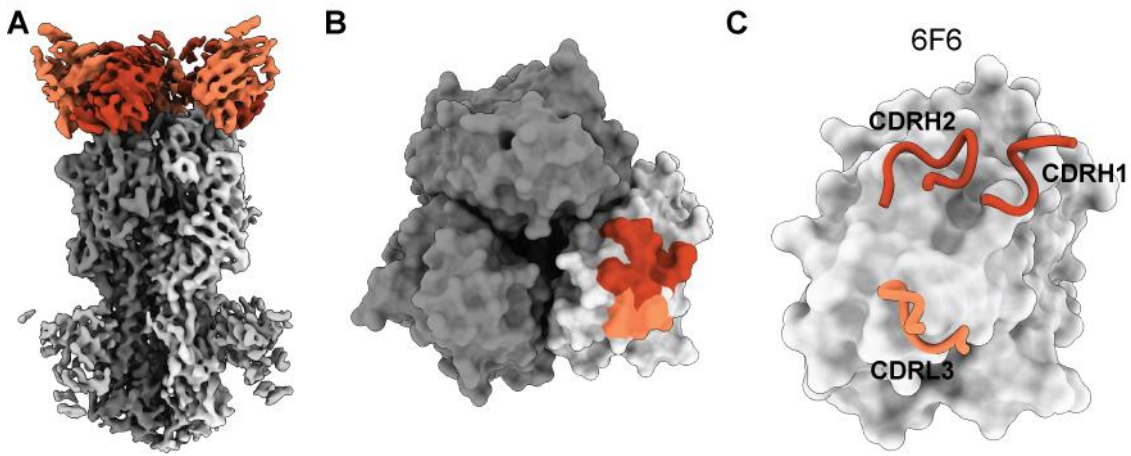

Figure S6: Map, footprint, and complementarity determining region usage for KL-H15-6F6 mAb. (A) Final KL-H15-6F6 EM map colored by proximity to A/wt shearwater/WA/2576/1979 H15 HA and KL-H15-6F6 Fv docked into density using ChimeraX. Light-chain depicted in light orange and heavy-chain depicted in burnt orange. (B) KL-H15-6F6 footprint on surface depiction of A/wt shearwater/WA/2576/1979 H15 HA. (C) CDRs involved in antigen engagement as demonstrated by EM map and GetContacts program (https://getcontacts.github.io/index.html, Table S2).

	KL-H15-3G11 + WA79 H15	KL-H15-6H4 + CR9114 + WA79 H15	KL-H15-6G8 + CR9114 + WA79 H15	07-5G01 + CR9114 + WA79 H15	KL-H15-6F6 + KL-H15-7B11 + WA79 H15
Access codes					
Grid Type	Quantafoil R 1.2/1.3 Cu 300	Quantafoil R 1.2/1.3 Cu 300	Quantafoil R 1.2/1.3 Cu 300	Quantafoil R 1.2/1.3 Cu 300	Quantafoil R 1.2/1.3 Cu 300
Freezing Conditions	RT, 100% humidity, blot force 1, 3uL of sample, 0.1% OBG	RT, 100% humidity, blot force 1, 3uL of sample, 0.1% OBG	RT, 100% humidity, blot force 1, 3uL of sample, 0.1% OBG	RT, 100% humidity, blot force 1, 3uL of sample, 0.1% OBG	RT, 100% humidity, blot force 1, 3uL of sample, 0.1% OBG
PDB	9P9Q	9P9R	9P9S	9P9T	-
EMDB	EMD-71419	EMD-71420	EMD-71421	EMD-71422	EMD-71424
Data collection and processing					
Microscope	Glacios	Krios	Krios	Krios	Glacios
Magnification	190,000	105,000	105,000	105,000	190,000
Voltage (kV)	200	300	300	300	200
Electron exposure ($e^-/Å^2$)	46.95	49.77	50.6	49.64	45.42
Defocus range (μm)	0.7-1.4	0.8-1.5	0.8-1.5	0.8-1.5	1-1.8
Pixel size (Å)	0.725	0.833	0.833	0.833	0.718
Detector	Falcon IV	Bioquantum K3	Bioquantum K3	Bioquantum K3	Falcon IV
Imposed Symmetry	C1	C1	C1	C3	C3
Final particle number	47,527	95,746	419900 (symmetry expanded)	92,304	166,675
Map resolution (Å)	3.70	3.14	3.41	3.33	3.34
FSC Threshold	0.143	0.143	0.143	0.143	0.143
Map sharpening B-factor ($Å^2$)	-73.9	-85.5	-98.7	-111.2	-71.7
Model refinement and validation					
Total Residues	1702	1723	1731	2178	
Amino-acids	1683	1711	1715	2160	
Carbohydrates	19	12	16	18	
RMSD Bonds	0.004	0.003	0.004	0.003	
RMSD Angles	0.682	0.571	0.672	0.62	
Ramachandran					
Outliers (%)	0.00	0.00	0.00	0.00	
Allowed (%)	7.76	5.98	6.55	8.17	
Favored (%)	92.24	94.02	93.45	91.83	
Rotamer outliers (%)	0.00	0.34	0.00	0.00	
Clash score	1.02	0.75	1.57	1.67	
Molprobity score	1.28	1.14	1.33	1.41	
FSC model (0/0.143/0.5)	3.6/3.7/4.1	3.0/3.1/3.5	3.0/3.1/3.4	3.2/3.3/3.6	
EMRinger score	1.95	3.05	2.90	2.74	

Table S1. Cryo-EM data collection, processing, model refinement and validation statistics. Validation statistics were generated using Phenix 1.21.2 Comprehensive Validation Tool (Barad et al., 2015; Chen et al., 2010).

KL-H15-6G8 + CR9114 + WA79 H15

H15	Heavy	Chain	Interaction
164	100	A	vdw
166	33	A	vdw, hbsb
166	56	A	vdw, hbss
167	52	A	vdw, hbss
168	100	A	vdw
168	99	A	vdw, hbsb
169	100	A	vdw, hbsb
169	99	A	vdw
171	100	A	vdw
202	54	A	vdw
206	97	A	vdw, hbss

H15	Light	Chain	Interaction
136	27	A	vdw, hbss
136	92	A	vdw, hbsb, hbss
136	93	A	vdw
137	92	A	vdw
137	93	A	vdw, hbsb
164	94	A	vdw
165	96	A	vdw
171	32	A	vdw
171	92	A	vdw, hp

KL-H15-3G11 + WA79 H15

H15	Heavy	Chain	Interaction
165	33	A	vdw
165	58	A	vdw
166	33	A	vdw, hbsb
167	52	A	vdw
167	54	A	vdw, hbss
168	100	A	vdw, hbsb
168	98	A	vdw
168	99	A	vdw, hbsb
169	100	A	vdw, hbsb
169	98	A	vdw, hbbb
171	100	A	vdw, hbsb
206	97	A	vdw

H15	Light	Chain	Interaction
136	92	A	vdw, hbsb
137	93	A	vdw
138	92	A	vdw, hp
164	92	A	vdw
165	94	A	vdw
171	32	A	vdw
171	92	A	vdw, hp
172	28	A	vdw, hbsb

07-5G01 + CR9114 + WA79 H15

H15	Heavy	Chain	Interaction
136	52	A	vdw
136	52A	A	vdw, hbss
136	53	A	vdw, hbsb
136	56	A	vdw
137	50	A	vdw
138	100D	A	vdw, hbsb
164	100D	A	vdw
164	58	A	vdw
168	47	A	vdw
168	58	A	vdw
169	58	A	vdw, hbsb
171	56	A	vdw
171	58	A	vdw
173	55	A	vdw
173	56	A	vdw

H15	Light	Chain	Interaction
139	32	A	vdw, pc
165	91	A	vdw
165	93	A	vdw
165	94	A	vdw
165	95	A	vdw

KL-H15-6H4 + CR9114 + WA79 H15

H15	Heavy	Chain	Interaction
136	53	A	vdw, hbsb
136	54	A	vdw, hbss
137	52	A	vdw, hbsb
164	52	A	vdw, hbss
165	31	A	vdw
167	97	A	vdw
167	99	A	vdw
168	33	A	vdw
168	97	A	vdw
169	33	A	vdw, hbsb, hp
171	52	A	vdw
172	56	A	vdw, hbsb
173	54	A	vdw
350	55	A	vdw

H15	Light	Chain	Interaction
197	27D	A	vdw
198	27E	A	vdw, hbss
198	27F	A	vdw
198	29	A	vdw, hbss
201	27E	A	vdw
201	32	A	vdw, hbss

172	27D	A	vdw
172	28	A	vdw, hbbb, hbsb
173	28	A	vdw
174	28	A	vdw, hbsb, hbss

172	29	A	vdw, hbsb
173	27D	A	vdw, hp
173	28	A	vdw
173	92	A	vdw, hp
174	28	A	vdw

165	96	A	vdw
166	91	A	vdw
166	92	A	vdw
167	94	A	vdw
168	94	A	vdw, hbsb, hbss

206	32	A	vdw
206	91	A	vdw, hbsb
207	92	A	vdw, hbbb

Table S2. Epitope-paratope contacts predicted from cryoEM models. The GetContacts program (https://getcontacts.github.io/index.html) was used to predict residue interactions at the epitope-paratope. Interactions are abbreviated as follows: van der Waals (vdw), side-chain to backbone hydrogen bonding (hbsb), backbone to backbone hydrogen bonding (hbbb), side-chain to side-chain hydrogen bonding (hbss), and hydrophobic (hp).